

# **NURail Project:**

## **NURail2017-UIC-R16**

The final report for NURail project: NURail2017-UIC-R16 consists of two distinct documents related to the project titled: “Coupled Multibody and Finite Element Analysis of Rail Substructure Behavior”.

1. Pages 2 – 32: “Analysis of Vibrations in a Structure due to Passing Trains Using a Coupled Finite Element and Multibody Dynamics Model” by Craig Foster.
2. Pages 33 – 68: “Computational Analysis of Railroad Ballast Settlement” by Craig Foster.

02-September-2020

Grant Number: DTRT13-G-UTC52



**National University Rail Center - NURail**  
US DOT OST-R Tier 1 University Transportation Center

NURail Project ID: NURail2017-UIC-R16a

**Analysis of Vibrations in a Structure due to Passing Trains Using a Coupled Finite Element and  
Multibody Dynamics Model**

By

Craig Foster  
Associate Professor  
Department of Civil and Materials Engineering  
University of Illinois at Chicago  
foster@uic.edu

29-08-2020

Grant Number: DTRT13-G-UTC52

## **DISCLAIMER**

Funding for this research was provided by the NURail Center, University of Illinois at Urbana - Champaign under Grant No. DTRT13-G-UTC52 of the U.S. Department of Transportation, Office of the Assistant Secretary for Research & Technology (OST-R), University Transportation Centers Program. The contents of this report reflect the views of the authors, who are responsible for the facts and the accuracy of the information presented herein. This document is disseminated under the sponsorship of the U.S. Department of Transportation's University Transportation Centers Program, in the interest of information exchange. The U.S. Government assumes no liability for the contents or use thereof.



## **TECHNICAL SUMMARY**

### **Title**

Analysis of Vibrations in a Structure due to Passing Trains Using a Coupled Finite Element and Multibody Dynamics Model

### **Introduction**

Vibration from trains can affect nearby structures, especially in urban areas. The first step toward mitigating vibration is to quantify them in a meaningful way. If vibrations can be predicted, then mitigation techniques can be applied during construction, if necessary. Different mitigation approaches can also be compared for effectiveness.

### **Approach and Methodology**

A finite element model is created of the substructure, including ballast, subballast, soil, and a nearby building. The finite element model is decomposed modally, and truncated modal information is fed into a multibody dynamics code. The multibody code analysis the dynamic response in the time domain. The modal displacements are used to reconstruct the displacements and accelerations in the building, which are then analyzed to determine whether comfort criteria are met.

### **Findings**

The simulation can predict realistic vibrations in buildings. The coupled model can make predictions in reasonable simulation times.

### **Conclusions**

With continued validation, the proposed method can be used to realistically predict vibrations and examine the effects of mitigation techniques on ground-borne vibrations.

### **Recommendations**

The model should be further validated on real soils. In reality, some dynamic testing of soils may be necessary in practice, as subsurface site conditions are difficult to know with accuracy. Building must also be characterized accurately

## **Publications**

S. Masurekar. 3D FEM & Multibody System Coupling of Railroad Dynamics with Vibration of Surrounding Building Structure. Masters Thesis. University of Illinois at Chicago.

## **Primary Contact**

### **Principal Investigator**

Craig Foster  
Associate Professor  
Department of Civil and Materials Engineering  
University of Illinois at Chicago  
(312) 996-8086  
foster@uic.edu

## **Other Faculty and Students Involved**

Sarvesh Masurekar  
Graduate Research Assistant  
Department of Civil and Materials Engineering  
University of Illinois at Chicago  
(312) 996-0438  
smasur2@uic.edu

Ahmed El-Ghandour  
Graduate Research Assistant  
Department of Civil and Materials Engineering  
University of Illinois at Chicago  
(312) 996-0438  
aelgha2@uic.edu

### **NURail Center**

217-244-4999  
[nurail@illinois.edu](mailto:nurail@illinois.edu)  
<http://www.nurailcenter.org/>

# **Analysis of Vibrations in a Structure due to Passing Trains Using a Coupled Finite Element and Multibody Dynamics Model**

## **ABSTRACT**

Ground-borne vibrations in structures due to passing trains are an ongoing issue in the rail industry. While in extreme cases such vibrations can lead to structural fatigue and failure, occupant comfort is usually the controlling factor. With the advent of higher-speed rail as well as the increasing value of urban real estate near train tracks, accurately predicting these vibrations becomes increasingly important. In this paper, we examine a coupled finite element and multibody dynamics approach to quantifying vibrations. Finite element software is used to generate the complex geometry and modes shapes which are fed into the multibody code, which simulates the passing train in the time domain. Reconstruction of the results from the mode shapes in the finite element software allows us to quantify accelerations in the building and other relevant quantities. An example problem is used to verify the approach.

**KEYWORDS:** Ground-borne vibrations, rail, multibody dynamics, finite elements, subgrade

## **1. INTRODUCTION**

Vibrations in buildings caused by passing trains have long been an issue in railway engineering, especially in urban areas [Lombaert, et al 2015]. Motion from passing trains can cause discomfort to building occupants, interfere with equipment, and in more severe cases structural degradation. A number of solutions have proposed to mitigate vibrations. However, in order to ensure they are effective enough, some prediction must be made as to magnitude of the acceleration.

Many empirical, analytical and numerical techniques have been applied to attempt to predict the response of a passing train. A relatively recent review of models of ground-borne vibration from trains is given in [Lombaert, et al 2015]. Analytical techniques are generally relatively straightforward to apply, but are difficult to apply to building vibration, especially when the geometry around the site is complex. They may treat the soil as a Winkler foundation [Chen and Huang, 2000] or a multilayered elastic half space [Krylov, et al 2000], and may include the effects of rail pads and sleepers [Kumawat et al 2019]. Empirical methods are also easy to apply, are based observations, and are therefore widely used. Both the US Federal Railroad Administration (FRA) and the Swiss Federal Railways (SBB) employ empirical models [Hanson, et al 2005, Hanson, et al 2006, Kuppelweiser and Ziegler, 1996]. However, because of the observational nature, they are not physics-based and are therefore to

extrapolate or sue to investigate mitigation techniques. Direct physical measurements can also be made, but these can be expensive and can only be made after the track is constructed for full accuracy.

With increasing computational power, numerical methods have been developed to reduce the expenses that come along with experimentation. The finite element method, with its flexibility in modeling different geometrical shapes, is the most common method. Due to issues with wave reflection, these methods often use infinite elements [Shih et al 2016], boundary elements [O'Brien and Rizos 2005, Galvin et al 2010a,b, Ghangale et al 2019], or other techniques at the boundary. Often, the simulation is split into two parts: first determining the source excitation from the passing train, and then propagation the waves through the substructure to the building [Lombaert, et al 2015, Kuo et al 2019]. Some models are fully three-dimensional (e.g. [Shih et al, 2016, Galvin, et al 2010b]), while so-called 2.5-dimensional models are popular due to their efficiency ([Ghangale et al 2019, Galvin, et al 2010a, Bian et al 2008], among others). Such models assume an infinitely long structure in the direction of the track, greatly reducing the number of elements necessary.

Multibody dynamics are extensively used in the rail industry for train and track analysis (e.g. [Shabana et al, 2007, Recuero et al 2011, El-Ghandour et al, 2016] among others). A new multibody system method was developed by Chamorro et al (2011) to model flexibility of the rail which was based on floating frame of reference formulation. This formulation was incorporated with MBS code to simulate the motion of railroad vehicles. El-Ghandour et al (2016) investigated the train substructure interaction under dynamic loading by using a coupled technique between finite element method and multibody dynamics. Also a bridge approach problem was investigated for problems due to the stiffness variation of the track from softer substructure to stiffer foundation on the bridge [El-Ghandour and Foster, 2019]. Many rolling contact theories have been put forward to calculate the tangential contact forces which are expressed as a function of the relative velocity between wheel and the rail and stiffness coefficients given in Kalker's table [Kalker, 1990]. Moncef Toumi et al. [Toumi et al 2016] developed a three-dimensional finite element model to study the frictional rail-wheel rolling contact with increased spin effect in elasticity with three different analyses: explicit dynamic, implicit quasi-static and implicit moderate energy dissipation analysis.

Multibody systems are less commonly used in vibration analysis of the substructure, which usually simplifies the applied loads, however. Rucker and Auersch (2007) used a multibody analysis to predict the vibrations on the track, but decoupled it from the ground vibration source and propagation finite element simulations. Kouroussis and Verlinden (2015) and Connolly et al (2019) also employed a decoupled simulation approach. A fully coupled co-simulation approach, which includes feedback between all components, is often considered computationally expensive.

Though not the focus of this investigation, a major challenge in analysis ground-borne vibrations is parameter determination. Soils are heterogeneous, complex materials, making it difficult to fully analyze any given site completely. Hybrid methods have shown promise in helping to evaluating sites [Kuo et al 2019, Kouroussis et al 2015, Kuo et al 2011]. These methods use limited experimental data

to calibrate uncertain parameters in the numerical models. Good hybrid methods, however, rely on sound underlying numerical models.

In this research, we use a coupled approach between finite element method and multibody dynamics to model the rail and the substructure below it that can inspect the wheel-rail interaction and determine the contact forces that give rise to the substructure deformations. Using modal decomposition of the substructure, the full geometry can be created in the finite element model, and building vibrations can be reconstructed in the postprocessing stage. We create a finite element model of the track system that include the geometry as well as the material properties of the rail, sleepers, fasteners, track substructure and a concrete framed building nearby. The model is built in commercially available FE ANSYS software using Mechanical ANSYS Parametric Design Language (MAPDL). Modal mass and stiffness data are then extracted after performing modal decomposition on the model and this information is then imported into a multibody software SAMS. The multibody system code is used to simulate the moving train over the rail structure and study the contact forces that are generated due to this interaction using a contact algorithm. The floating frame of reference technique was used to formulate the forces in the simulation driven by multibody code. The FFR technique formulated by Shabana et al. (2007) analyzes the dynamics of a multibody system which undergoes small strains and large relative rotations. Here, in this research the techniques adopted by El-Ghandour et al (2016) were used but they were further extended to calculate the nodal displacements and nodal accelerations from the corresponding modal values. Subsequently, the strains and stresses were also determined in the substructure. This research is used to investigate the vibrations in the nearby building by using a coupled 3D FEM and MBS model of the railroad system.

The remainder of this paper is organized as follows: Section 2 discusses the creation of finite element model of the rail, substructure and the building in Mechanical ANSYS APDL. Section 3 outlines the modal analysis performed on the model to extract modal information. Section 4 discusses the multibody dynamic analysis and formulations used in this system. Section 5 explains how the results are reconstructed back into the finite element software after calculating it in MATLAB. Section 6 analyzes a numerical example and the results obtained for the analysis, and finally Section 7 summarizes the paper.

## **2. FINITE ELEMENT MODEL**



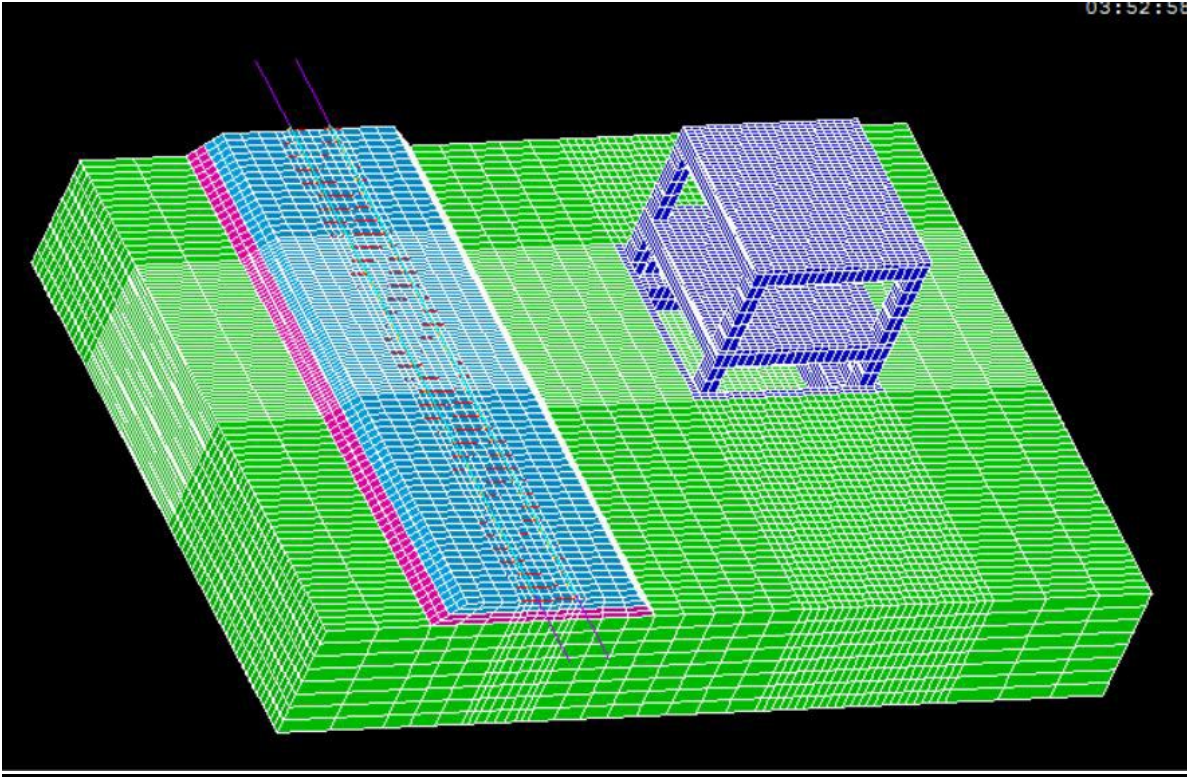


*Figure 1: FE model of the entire rail system with an adjacent building structure*

Using the finite element software package ANSYS APDL, we build a 3D model of the rails, sleepers, fasteners that connect them together and the substructure beneath the rail assembly including the ballast, subballast and the subgrade, shown in Figure (1). We also model a two-story concrete building in the vicinity of the rail system. The rails and the sleepers are modeled using three dimensional beam elements (BEAM 188). The three substructure layers of ballast, subballast, the subgrade and the concrete building are all modeled using 8-node hexahedral brick element (SOLID185). Spring-damper elements (COMBIN14) are used to model the fasteners and rail pads that connect the deformable rail with the sleepers and help ease off the deformation between rail and sleepers. The modal damping coefficient values used for this model was 3% as this roughly reflects the damping in the soil that dominates the geometry.

As the sleepers, modeled using beam elements, are connected to the solid brick elements, the torsional degrees of freedom associated with them are constrained, following El Ghandour and Foster (2019). The rail track is divided into two sections: a rigid section and a deformable section (Figure (2)). The rigid section is designed to form a track before and after the deformable part of the rail. It has all its degrees of freedom constrained. This approach helps to minimize to avoid the initial sudden impact of the wheelset which is dropped from a small distance initially and an unwanted sharp noise in the analysis at the beginning of the simulation.

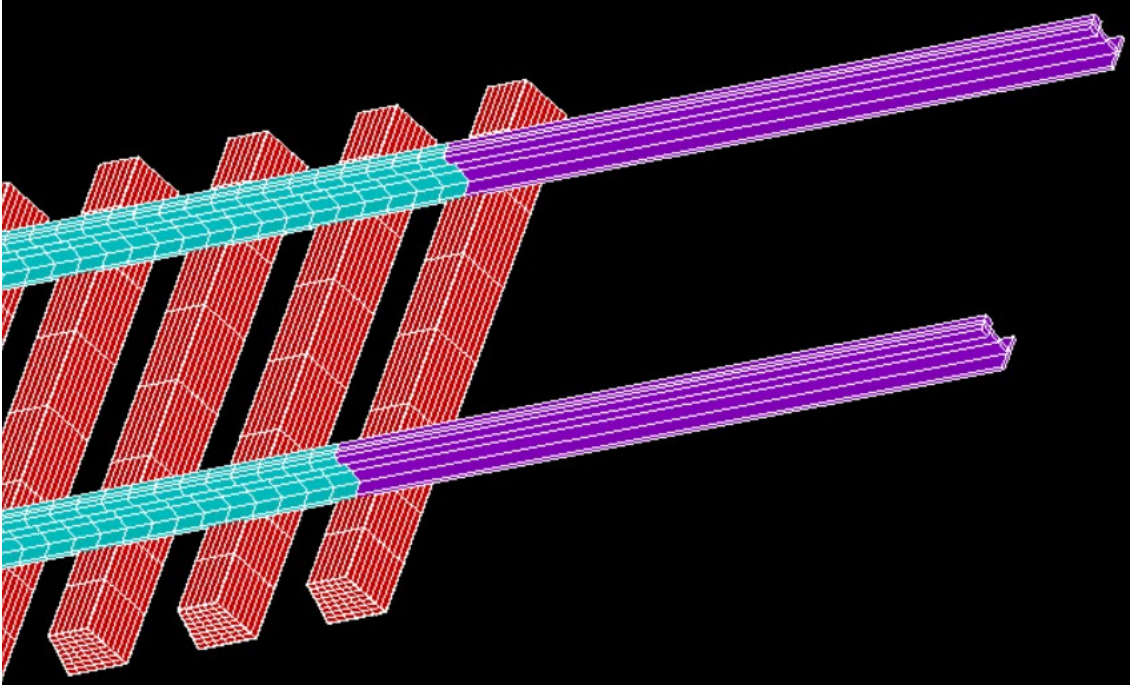


*Figure 2:3D view of the FE model of the rail and sleepers showing transition from rigid to flexible.*

The subgrade is constrained on all sides perpendicular to the boundaries to avoid out of plane motion. The bottom side of the subgrade is fully fixed and constrained for all degrees of freedom to make sure it is consistent with the physical behavior of the soil and its attachment with the hard rock below it. A two story building structure of height 8.2 meters with 7.2 m x 7.2 m length and width is made of concrete. Also to ensure stability of the building, it has a foundation of 2.4 meters below the substructure level firmly standing on four 1.2 x 1.2 x 1.2-meter high flexible footings forming the base of this building. The foundation has concrete wall of 2.4 meters surrounding its basement level from all the four directions which helps to keep the soil in place around the building.

The extent boundary has been tested to ensure that wave reflection is not an issue. Details of this testing are presented in Masurekar (2019), but are omitted here for brevity.

### **3. MODAL ANALYSIS**

In this research, we used the modal superposition method for linear dynamic analysis to calculate and superimpose individual vibration mode shapes of the rail and building model to calculate the displacement and acceleration time history. For rail vibrations in buildings, the principal interest is the building acceleration. Usually a small number of mode shapes of the lower order frequencies dominate

the motion. However, due to the nature of the relatively concentrated, moving load of the wheel-rail contact, the number of mode shapes required in the rail dynamics case is larger than in many problems [El-Ghandour et al 2016]. In this case, roughly 300 modes are required for convergence, two of which are shown in Figures 3 and 4. While relatively high compared to some problems, these 300 modes are still much smaller than the thousands of degrees of freedom in the finite element model. In our model of the three-dimensional railroad structure, we perform modal analysis to generate the mode shapes and fundamental frequencies. The modal mass matrix and the stiffness values are extracted when we run the modal analysis for the entire model. This information taken from the modal analysis is then used as input parameters and used to run the multibody dynamic analysis in the time domain.

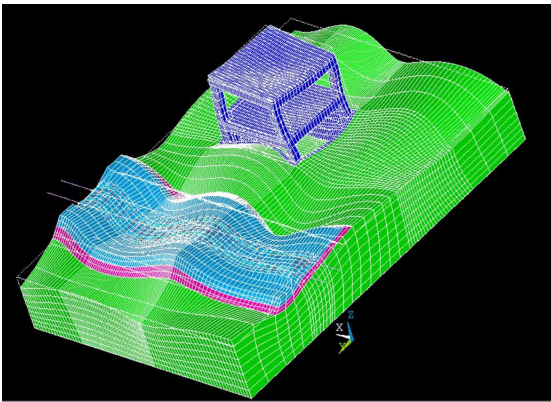


*Figure 3: A deformed shape of a lower mode at a mode at frequency of 22 Hz*

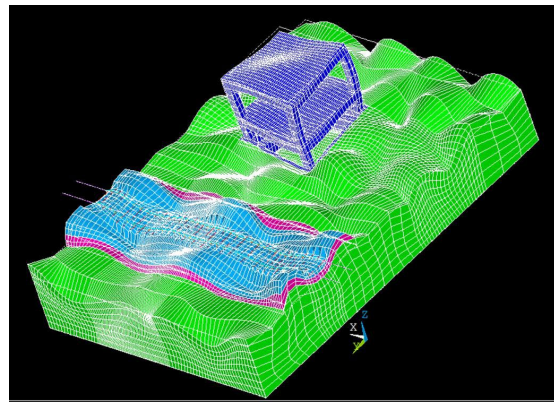


*Figure 4: A deformed shape of a lower mode at a frequency of 45 Hz*

Further investigating rail induced vibrations, we have extracted 300 modes for our problem. While extracting the modes, it ensured that all mode shapes covered deformation in all directions, as well as torsional. The frequency range for the extracted modes in our example is between 9.56 Hz and 57.87 Hz. The modal analysis data is fed to the multibody dynamic code to perform the simulation in SAMS (Simulation of Articulated Mechanical System Software). This data has to be altered according to the input format that is accepted by it. This information is first read by the pre-processing code PreSAMS to feed the nodal mass into the multibody dynamics code. The degrees of freedom that are associated directly with the rail geometry only are considered and rest of them are eliminated by a nodal elimination technique.

#### **4. MULTIBODY DYNAMICS MODEL**

The dynamic analysis for the rail-wheel interaction, using the modal information from the finite element program, is run to find the wheelset displacement, wheel-rail contact forces and the modal

displacements for the rail system. To determine the displacement of the bodies over the rail substructure in this research, we use the floating frame of reference technique. This technique was adopted by El-Ghandour et al (2016) and Recuero et al (2011) as well in their research to examine the performance of rail and wheel interaction, though Recuero used a simplified spring-damper model for the substructure.

The floating frame of reference (FFR) technique is a finite element formulation method that utilizes non-isoparametric elements to describe rigid body motion and small deformation of a system. This technique is not suitable for large deformations, but large relative rotations between separate bodies are permissible. With regards to the current problem of interest, the floating frame of reference formulation can be used since the deformations are small and hence we can get proper results. It is important that the element shape functions used in floating frame of reference finite element formulation method express arbitrary rigid body translations and rotations in all directions. Within FFR formulation, it is possible to reduce number of degrees of freedom in individual bodies using modal analysis. This approach effectively reduces the body to a set of desired mode shapes with many fewer degrees of freedom. The deformation of the flexible bodies in the multibody system can then be easily determined using this reduced model. The motion of each component, for example the suspended wheelset, is described with respect to the absolute fixed frame of reference. Each of the rails is defined by two interconnected models, the geometric model and the finite element model.

**4.1 The nodal elimination technique used for coupling:**

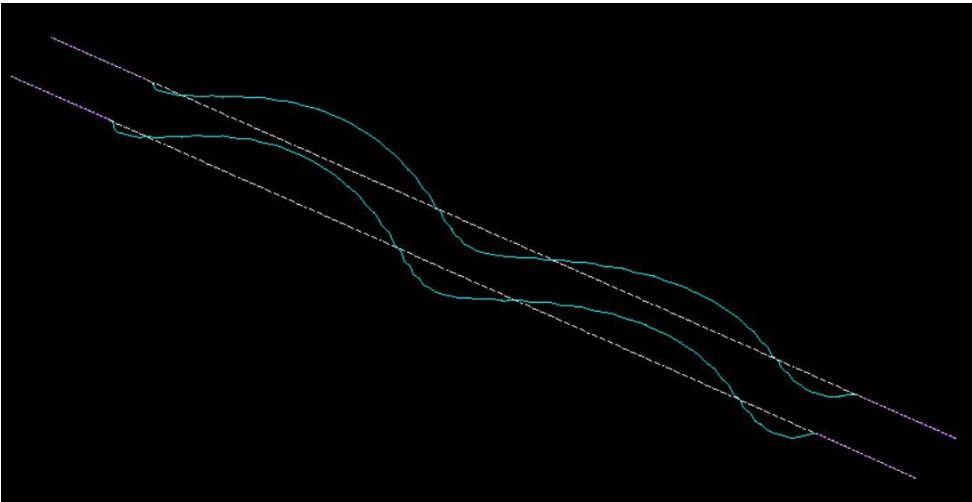


*Figure 5: Mode shape of the rail only at a lower frequency of 15 Hz*

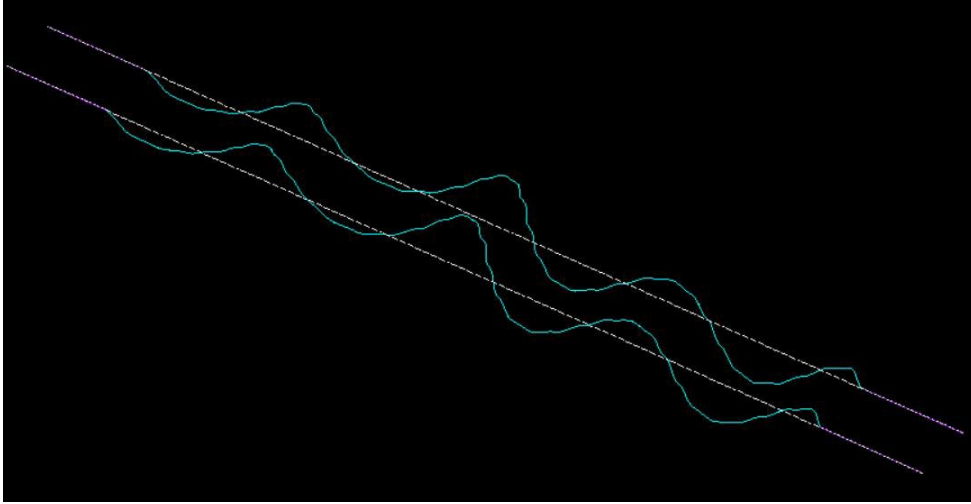


*Figure 6: Mode shape of the rail only at a higher frequency of 52 Hz*

After performing the modal analysis for the track and substructure, a nodal elimination technique was used to further improve the efficiency of the multibody simulation. After the modal decomposition, the mode shapes are truncated to include only the degrees of freedom corresponding to the rail nodes, as these are the only nodes needed for the multibody simulation [El-Ghandour et al 2016, El-Ghandour and Foster 2019]. The mode shapes for two modes are shown in Figures 5 and 6. This method helps in reducing the size of the mode shape vectors. It should, of course, be ensured that appropriate number of modes are extracted for the system to cover all kinds of expected displacement patterns in the body. Modal analysis and nodal elimination are very economical when it comes to the computation cost in the linear case. After nodal elimination technique is performed to shrink the data for entire system down to only the rail nodes, the dynamic analysis is performed on a Multibody package SAMS.

#### **4.2 Wheel-rail interaction in SAMS:**

Multibody system analysis is well suited to modeling dynamics of contact between rail and wheel, and SAMS has been developed to evaluate and study this interaction. The multibody code takes into account the time-dependent force conditions.

Many simplified techniques have been put forward in research papers to evaluate the contact forces and trace the contact path between two interacting bodies. In their research, Meli and Pugi (2013) approximated the contact position by using the linear superposition principle. They used the Elastic Contact Formulation for Algebraic Equations (ECFA) approach given by Shabana (2005) to determine

the contact point location. This technique allows the wheel to have six degrees of freedom with respect to the rail since it does not treat the governing equations as constraints. Small penetrations and separations between the rail and the wheelset are allowed in this algorithm, which is not exact but can approximate the contact very well. The surface contact is defined in terms of two non-generalized coordinates which are also known as surface parameters. This method of using parameters to locate any point on a contact surface simplifies the problem. The following four equations given by Shabana et al (2007) usually solved iteratively gives the contact point location for a wheel rail pair:

$$\mathbf{E}(s) = [\mathbf{t}_1^r \cdot \mathbf{r}^{wr} \quad \mathbf{t}_2^r \cdot \mathbf{r}^{wr} \quad \mathbf{t}_1^w \cdot \mathbf{n}^r \quad \mathbf{t}_2^w \cdot \mathbf{n}^r]^T = \mathbf{0}$$

Here  $\mathbf{E}(s)$  represents the contact point location,  $\mathbf{t}_i^j$  is the tangent vector of surface  $j$  with respect to surface parameter  $i$ ,  $\mathbf{r}^{wr}$  is the relative position of the contact point on the wheel with respect to the rail and  $\mathbf{n}^r$  is the normal vector at the point of contact on the rail.

The solution for the equation should be tested for a contact or small separation. This is calculated by determining the value of  $\delta$  from the equation  $\delta = \mathbf{r}^{wr} \cdot \mathbf{n}^r$ , where a positive value indicates separation between the rail and wheel and a negative value means that there is penetration. If the value of  $\delta$  is negative implying that there is contact between the rail and the wheel, then the normal force is calculated as per the formula  $F^N = -K_H \delta^{3/2} - C \dot{\delta} |\delta|$ ,

where  $F^N$  is the normal force,  $K_H$  is the Hertzian constant,  $C$  is the damping constant and  $\dot{\delta}$  is the time derivative of the penetration value. On the basis of Kalker's (2009) theory, Shabana et al. (2007) formulated a procedure to compute dimensions of the Hertzian contact ellipse, tangential and spin creepages and thereby the tangential creep forces and creep spin moment. To take into consideration the rail deformation effect on the determination of the contact point, the element that is in contact has to be determined first and subsequently the rail geometry is updated by an iterative process which is further used in the calculation of the tangential and spin creepages at the corresponding Hertzian contact patch.

### 4.3 Modal forces:

The mathematical formulation derived by Shabana et al (2007) that determines the relation between the modal forces and the nodal contact forces is solved by SAMS:

$$(\mathbf{Q}_e)_f = \Psi(i)^t \mathbf{f}$$

where  $\mathbf{f}$  is the nodal force which is applied on the rail nodes,  $\Psi(i)^t$  is the  $i^{\text{th}}$  generalized eigenvector which is extracted from the finite element model, and  $(\mathbf{Q}_e)_f$  is modal force which has to be calculated.

The nodal force applied on the nodes is represented as a vector form given below:

$$\mathbf{f} = \begin{Bmatrix} \mathbf{f}_r \\ \mathbf{f}_o \end{Bmatrix}$$

where force on the nodes that are not on the rail and are not considered for the simulation and eliminated are represented as  $\mathbf{f}_o$  and the force on the nodes that are a part of the rail and considered for the multibody analysis is represented by  $\mathbf{f}_r$ . Since in this scenario, the forces on the nodes that are not on the rail are zero, it is ignored and only  $\mathbf{f}_r$  is used for further computation. Thus, the equation is simplified to:

$$(\mathbf{Q}_e)_f = \Psi_r (i)^t \mathbf{f}_r,$$

where  $\Psi_r (i)$  is the eigenvector reduced down to only the rail nodes. After computing the modal forces, the next step is the calculation of the modal displacements, modal velocities and the modal accelerations by solving equations of motion.

#### **4.4 Equations of motion:**

The augmented form of the multibody equations derived by Shabana et al. (2007) are used in this research. Differential and non-linear algebraic constraint equations are simultaneously solved in this augmented method to find the solutions for the equations of motion. This augmented equation is given as:

$$\begin{bmatrix} \mathbf{m}_{rr} & \mathbf{m}_{rf} \\ \mathbf{m}_{fr} & \mathbf{m}_{ff} \end{bmatrix} \begin{bmatrix} \ddot{\mathbf{q}}_r \\ \ddot{\mathbf{q}}_f \end{bmatrix} = \begin{bmatrix} (\mathbf{Q}_e)_r \\ (\mathbf{Q}_e)_f \end{bmatrix} + \begin{bmatrix} (\mathbf{Q}_v)_r \\ (\mathbf{Q}_v)_f \end{bmatrix} - \begin{bmatrix} \mathbf{C}_{q_r}^T \\ \mathbf{C}_{q_f}^T \end{bmatrix} \lambda - \begin{bmatrix} \mathbf{0} \\ \mathbf{K}_{ff} \mathbf{q}_f \end{bmatrix}$$

where  $\mathbf{m}_{rr}$  is the inertia matrix for reference coordinates,  $\mathbf{m}_{rf}$  and  $\mathbf{m}_{fr}$  are the inertia matrices that dynamically couple elastic and reference coordinates,  $\mathbf{q}_f$  is the elastic modal coordinates vector that represents track and substructure in the flexible floating frame reference formulation while  $\mathbf{q}_r$  is the rigid body coordinates vector.  $(\mathbf{Q}_e)_r$  and  $(\mathbf{Q}_e)_f$  are the generalized external forces vectors in the rigid and elastic coordinates respectively,  $(\mathbf{Q}_v)_r$  and  $(\mathbf{Q}_v)_f$  represent the quadratic velocity inertia forces vector in rigid and elastic coordinates respectively,  $\mathbf{C}_{q_r}$  and  $\mathbf{C}_{q_f}$  are the Jacobian matrices as a result of the constraints for the rigid and elastic coordinates respectively,  $\mathbf{K}_{ff}$  is the stiffness matrix of the rail track and  $\lambda$  is the vector of Lagrange multipliers. A sparse matrix solver is used in multibody system to solve for reference and elastic accelerations to improve simulation speeds. Integration is performed in the time domain using an explicit Adams-Bashforth method [Shampine and Gordon, 1975].

## 5 RECONSTRUCTION OF RESULTS

We are studying the response of the entire substructure by reconstructing the nodal displacements from the modal data. Also, by further measuring the nodal accelerations, we study the discomfort that is being caused to the occupants due to the impact of the pressure and longitudinal waves on the building. The parameter that we are focusing on is acceleration at various sections of the building structure such as the flexible footing and different levels of columns and slabs.

The nodal displacements and accelerations is calculated from the modal results as:

$$\mathbf{U}_f = \Psi(i)^t \mathbf{q}_f$$

$$\ddot{\mathbf{U}}_f = \Psi(i)^t \ddot{\mathbf{q}}_f$$

where  $\Psi(i)^t$  is the matrix for the 300 mode shapes of the whole structure that were extracted during modal analysis,  $\mathbf{q}_f$  and  $\dot{\mathbf{q}}_f$  are the modal displacement and modal acceleration vectors obtained from the MBS code as output and  $\mathbf{U}_f$  and  $\dot{\mathbf{U}}_f$  are the nodal displacement and nodal acceleration vectors of the whole structure. The computation of these nodal displacements and acceleration from their respective modal parameters extracted from the multibody code is performed in MATLAB and then, using ANSYS APDL, it is reconstructed over each and every node of the model. Once the displacements are calculated, the elastic stress and strain values can be determined. With the nodal velocities, damping stresses may also be calculated.

## 6 NUMERICAL EXAMPLE

### Input data

The physical model of the substructure and building used in this research is a three-dimensional system of rail, sleepers, fasteners, ballast, subballast and subgrade. In our model, the soil is extended to the area surrounding the nearby building.



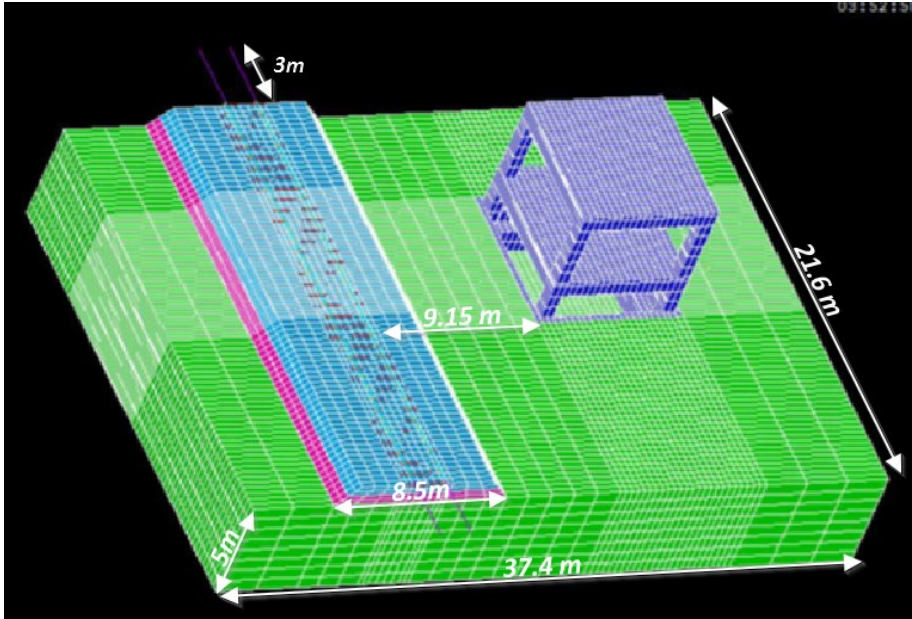
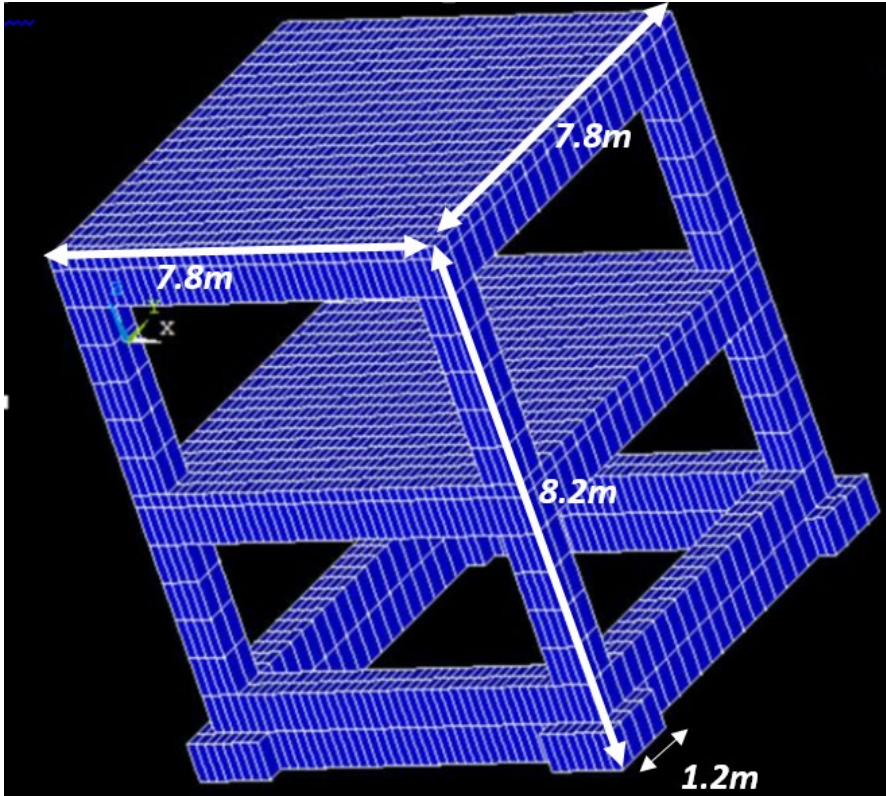


*Figure 7: Geometry of the finite element model*

The geometry of the finite element model with the structure is shown in Figure 7. The building is a two-story concrete structure (Figure (8)) with a half basement. The building is 7.8 x 7.8 m and is 8.2 m high. It is supported on 1.2 x 1.2 x 1.2 m flexible footings. A concrete basement wall also surrounds the structure to ground level to support the soil pressure. The material properties used in the finite element model are shown in Table 1.

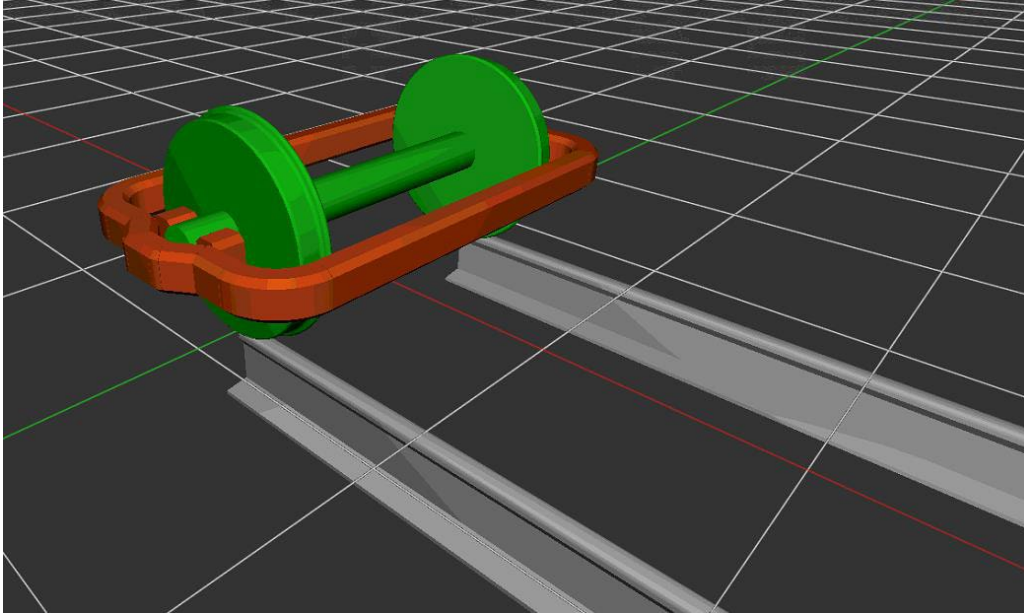
<b>Description</b>	<b>Value</b>	<b>Unit</b>
Length of the rigid rail	3	m
Length of the flexible rail	21.6	m
Gauge length	1.5113	m
Stiffness of the rail	210e9	N/m <sup>2</sup>
Density of the rail	7700	kg/m <sup>3</sup>
Poisson's ratio of the rail	0.3	
Cross-sectional area of the rail	64.5e-4	m <sup>2</sup>
Second moment of inertia of the rail-I <sub>yy</sub>	2010e-8	m <sup>4</sup>
Second moment of inertia of the rail-I <sub>zz</sub>	326e-8	m <sup>4</sup>
Timoshenko shear coefficient for the rail	0.34	
Length of a sleeper Length	2.5	m
Gap between sleepers	0.6	m
Stiffness of a sleepers	64e9	N/m <sup>2</sup>
Density of a sleeper	2750	kg/m <sup>3</sup>
Stiffness coefficient of a pad	26.5e7	N/m
Damping coefficient of a pad	4.6e4	N.s/m
Poisson's ratio of a sleeper	0.25	
Cross-sectional area of a sleeper	513.8e-4	m <sup>2</sup>
Second moment of inertia of a sleeper	18907e-8	m <sup>4</sup>
Timoshenko shear coefficient for a sleeper	0.83	
Stiffness of the ballast	260e6	N/m <sup>2</sup>
Density of the ballast	1300	kg/m <sup>3</sup>
Poisson's ratio of the ballast	0.3	
Stiffness of the subballast	200e6	N/m <sup>2</sup>
Density of the subballast	1850	kg/m <sup>3</sup>
Poisson's ratio of the subballast	0.35	
Stiffness of the subgrade	200e6	N/m <sup>2</sup>
Density of the subgrade	1850	kg/m <sup>3</sup>
Poisson's ratio of the subgrade	0.35	
Ballast depth	4.8	m
Subballast depth	0.5	m
Subgrade depth	0.5	m
Density of the concrete building	2500	kg/m <sup>3</sup>
Poisson's ratio of the concrete building	0.25	
Stiffness of the concrete building	31e9	N/m <sup>2</sup>
Height of the building	8.2	m
Width of the building	7.2	m
Perpendicular Distance between rail and building	9.15	m

Table I: Finite element model dimensions and material properties



*Figure 8: Dimensions of the building structure*

A suspended wheelset, shown in Figure (9), is run across the track, entering from the rigid section. The wheelset has flexible springs and is equivalent to the one described in [El-Ghandour and Foster 2019]. The simulation mimics vibrations set off from a transition from a stiff area to a flexible one. The analysis is made for an average speed of a train with the wheelset moving at 30 m/s, which is approximately 67 miles per hour. The material and geometrical parameters of the wheelset are shown in Table 2.



*Figure 9: Suspended wheelset model used in SAMS*

<b>Description</b>	<b>Value</b>	<b>Unit</b>
Mass	1568	kg
I <sub>xx</sub>	656	kg.m <sup>2</sup>
I <sub>yy</sub>	168	kg.m <sup>2</sup>
I <sub>zz</sub>	656	kg.m <sup>2</sup>
K <sub>t1</sub> =k <sub>t2</sub>	13500	N/m
K <sub>r1</sub> =k <sub>r2</sub>	25000	N/m
c <sub>t1</sub> =c <sub>t2</sub>	1000	N.s/m
c <sub>r1</sub> =c <sub>r2</sub>	0	N.s/m

*Table 2: Mechanical properties of the wheelset used in SAMS*

## 7 RESULTS

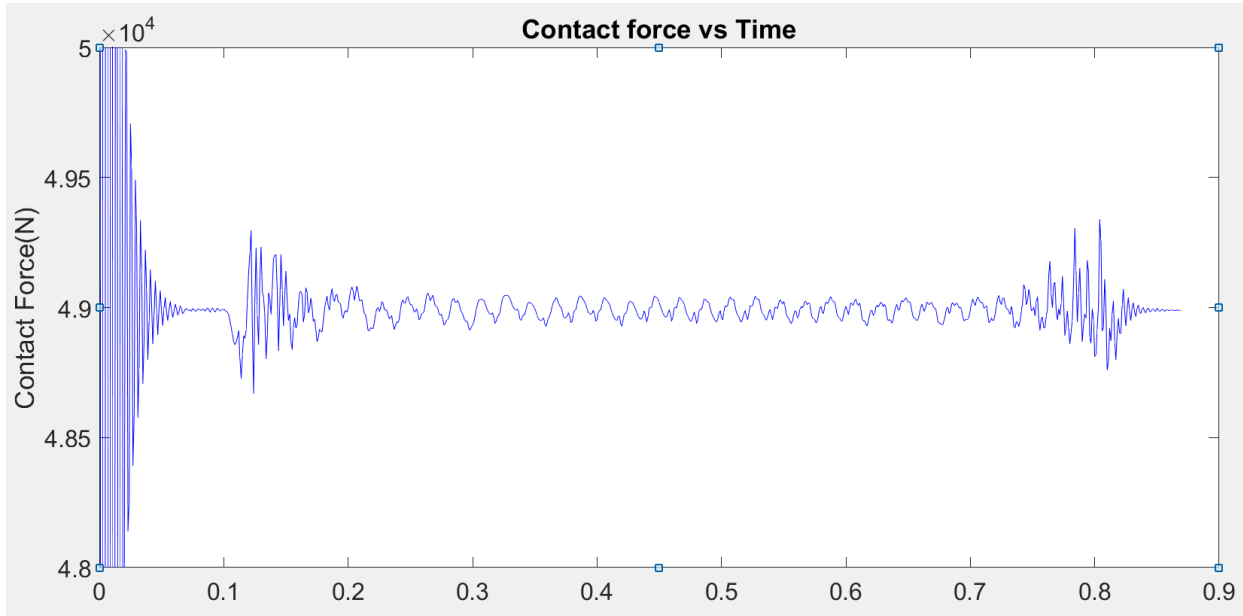


*Figure 10: Normal contact forces on the rail nodes due to the moving wheelset*

The contact forces that are applied on the rail by the suspended wheelset are shown in the Figure (10). The large initial values are vibrations of the wheelset as it is virtually dropped onto the rigid portion of the track. After settling out, there is a second peak as the wheelset moves from the rigid to flexible portion of the track. A third peak occurs when the wheelset leaves the flexible portion of the track to the rigid track at the far end of the simulation

### **Displacement, Stress and strain in the substructure and building:**

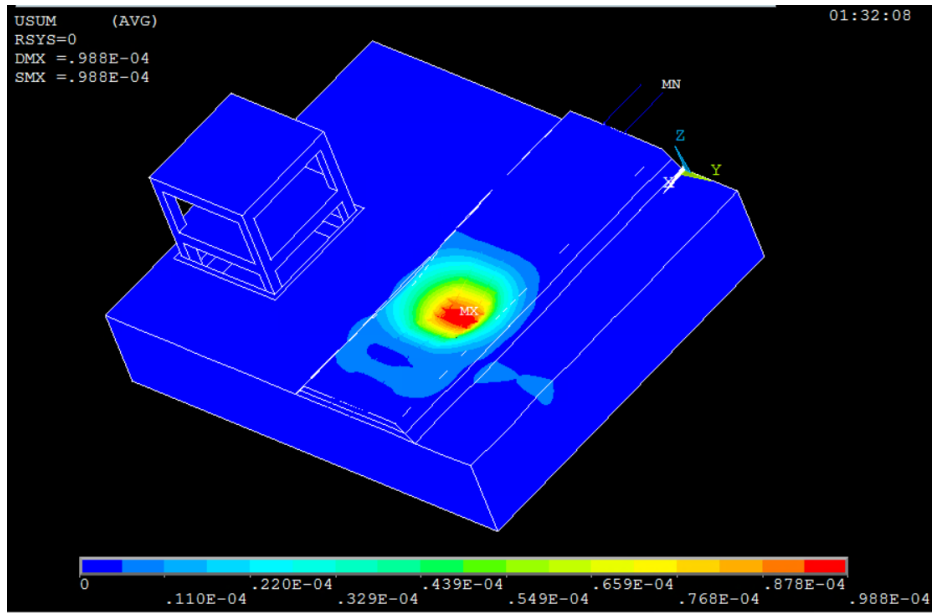


Figure 11: Displacement magnitude at the ballast and the subballast at time  $t = 0.54$  s from the start of the wheel-rail contact.

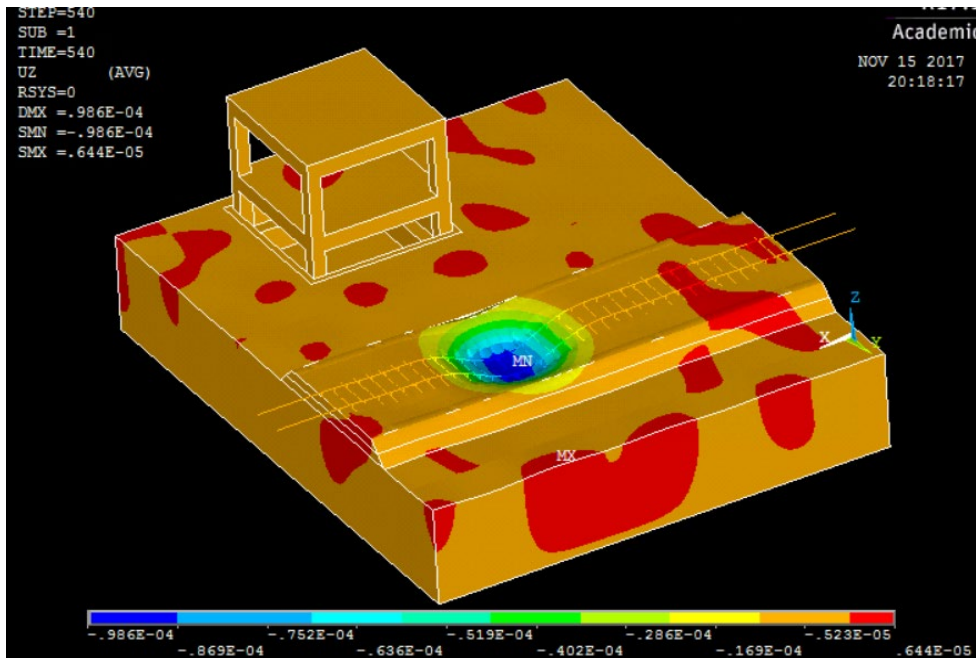


Figure 12: Z-Displacement at the ballast and the subballast at time  $t = 0.54$  s from the start of the wheel-rail contact.

The reconstructed values of magnitude of the displacements are shown in Figure (11), while the vertical displacement is shown in Figures (12). At this particular time step for which the nodal displacement contour is being plotted on ANSYS, the train is in line with the building structure. It is observed that the maximum displacement is experienced at the ballast due to the effect of moving contact forces on the rail and the sleepers. The weight of the moving suspended wheelset causes maximum vertical deflection as it moves over the rail in the region near the ballast and subballast. The rail and ballast are observed to experience comparatively larger displacement as compared to the building structure as the forces are more concentrated here. The maximum longitudinal displacement at the building is  $0.528 \times 10^{-5}$  m while the transverse displacement is  $0.283 \times 10^{-5}$  m. It is also observed, however small the displacement values are, that they are greater in the longitudinal direction at the building structure than in the transverse directions and the vibrations are transmitted through the substructure to the building.

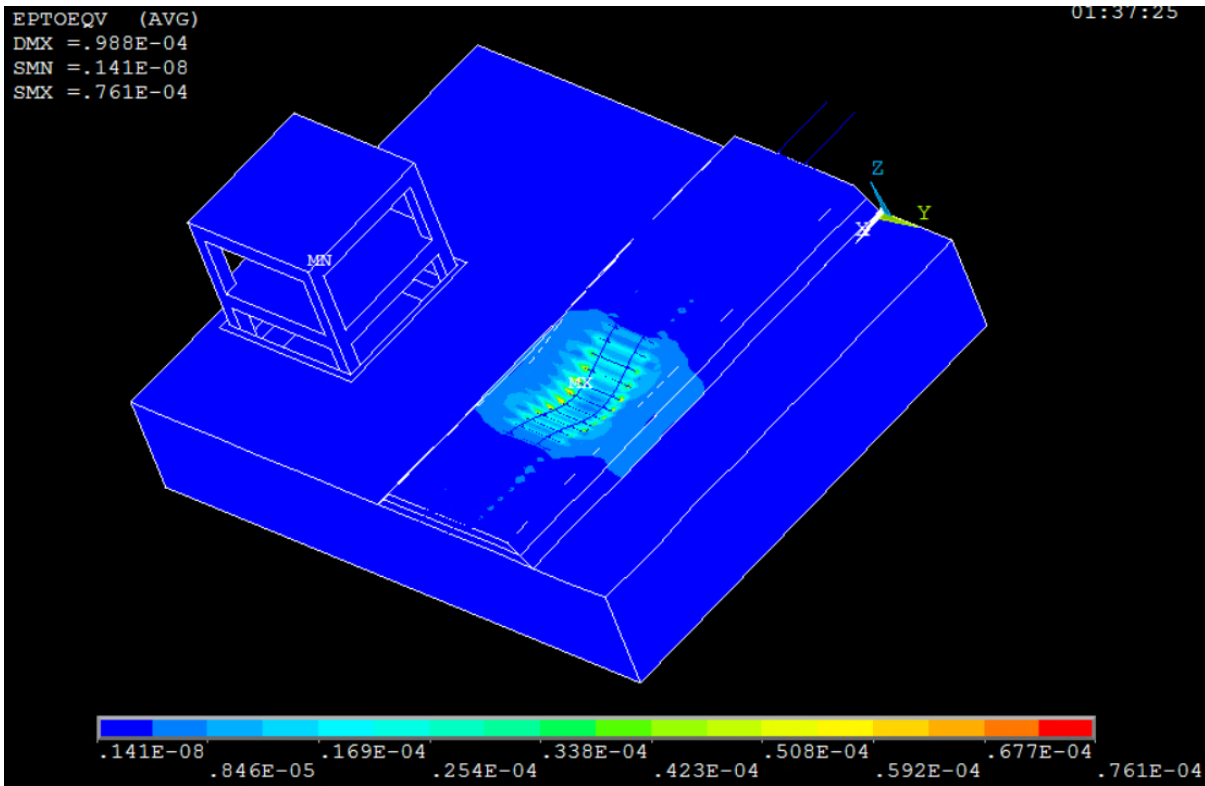


Figure 13: Equivalent strain at the ballast and the subballast at time  $t = 0.54$  s from the start of the wheel-rail contact.

The equivalent strain of the substructure is shown in Figure (13). Strain values are obviously highest near the wheelset contact area. Similarly, von Mises stress, shown in Figure (14) is largest near contact area. We can see some higher stresses in the stiffer structure, however, as it undergoes vibration.

Stresses can be seen in the range of 3580 to 4170 N/m<sup>2</sup> on the first floor. These are not high enough to be of structural concern, but do indicate that the vibration has some effect on the building.

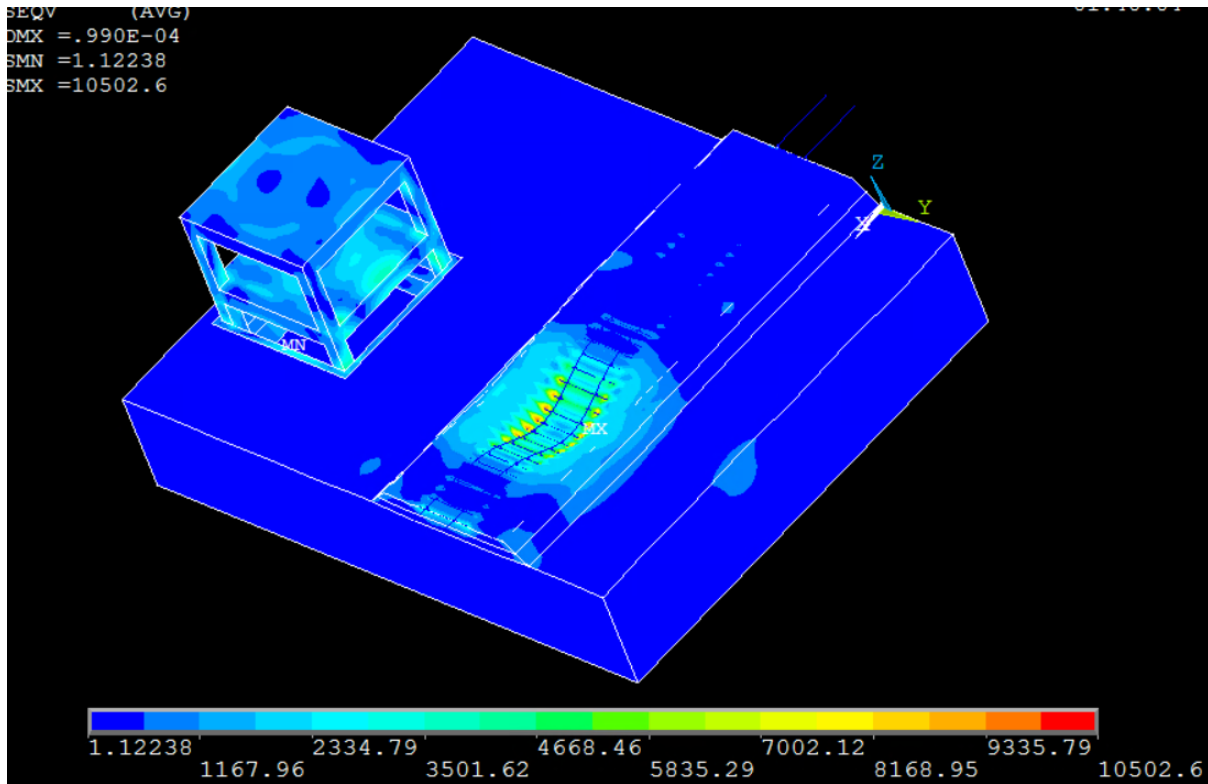


Figure 12: von Mises stress observed at the ballast, subballast and the building structure at time  $t=0.61$  seconds from the start of the wheel-rail contact.

### Check for occupant discomfort

Occupants may be present on the slab at level 1 and level 2 and there is a higher possibility of feeling vibrations in this region, we examine the total acceleration values at these two places of the building. The components of the acceleration are shown in Figures 15-17



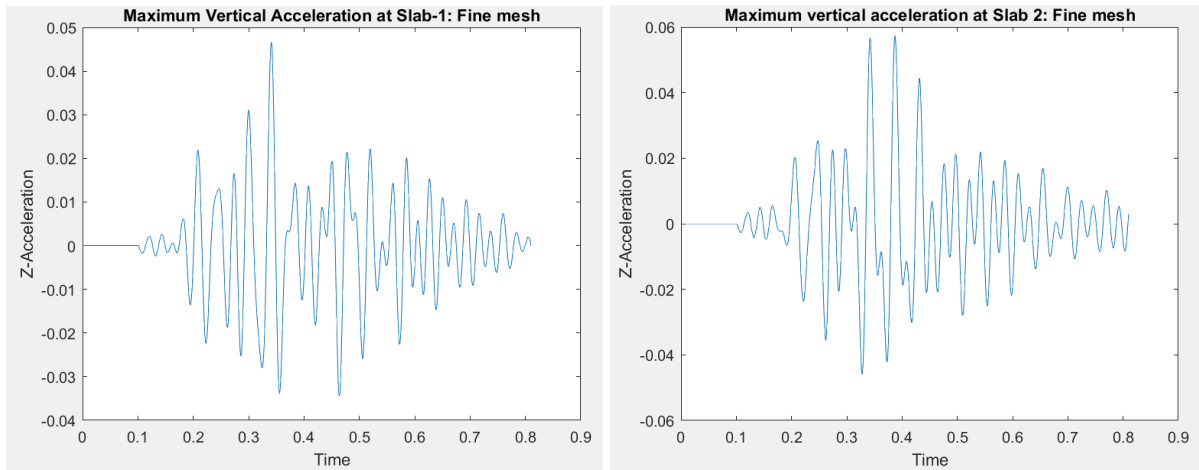


Figure13. Vertical acceleration of the floor slabs on the first (left) and second (right) floors.

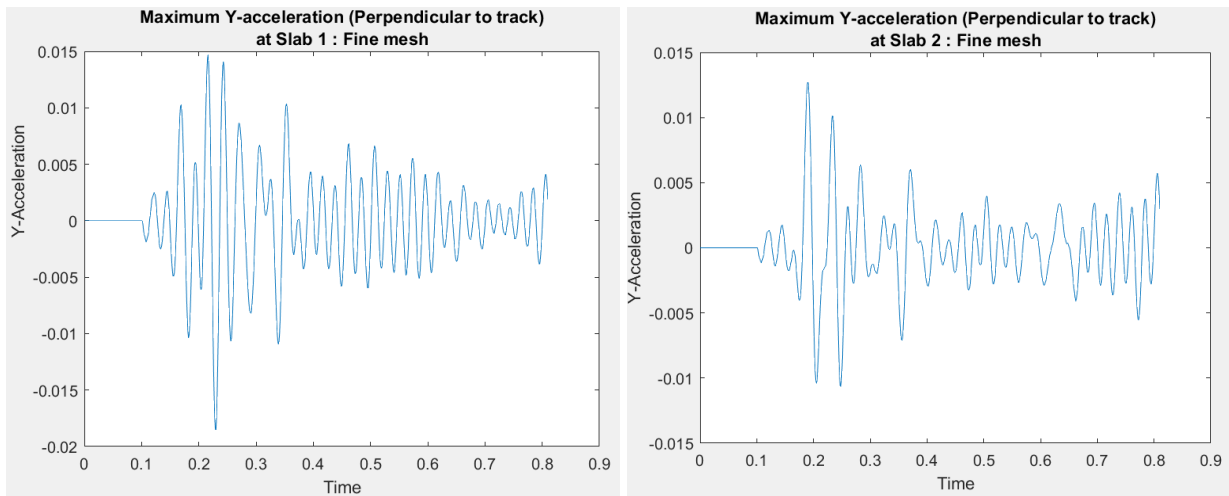


Figure 14. Y-acceleration (perpendicular to track direction) of the first floor slab (left) and second-floor slab

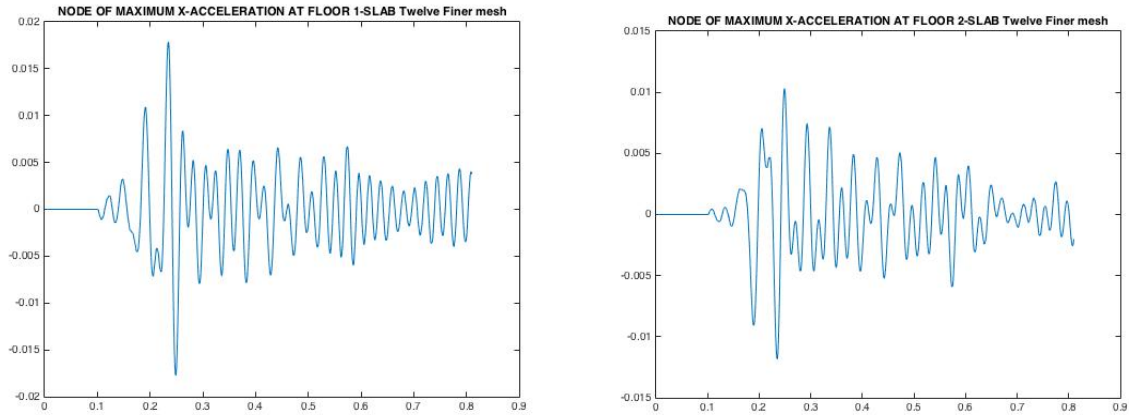


Figure 15. X-acceleration (parallel to track) of the first-floor slab (left) and second-floor slab (right).

The vertical acceleration is the largest component, which is intuitive as these are the largest motions caused by the wheelset. The other two components of the acceleration are roughly equal. The second floor experiences slightly higher accelerations than the first in this case.

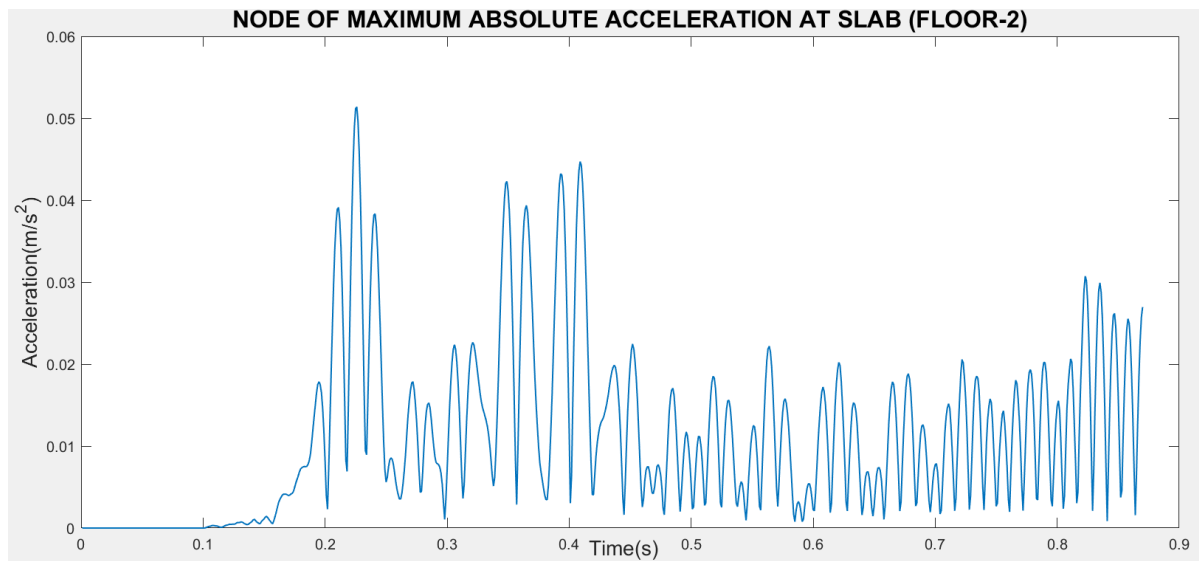
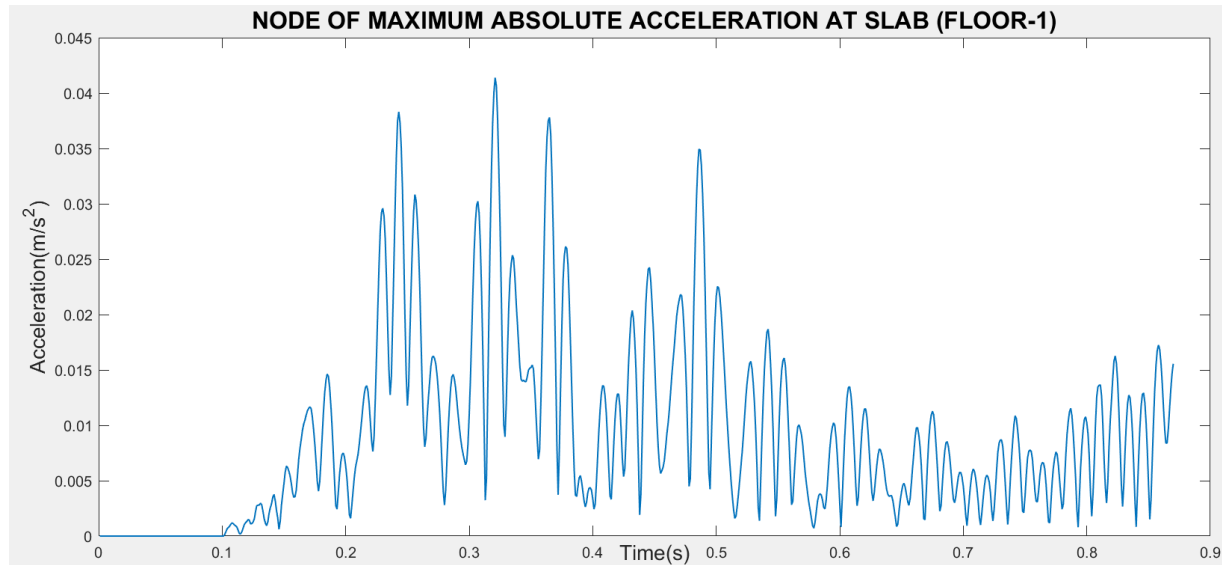


Figure 18: Magnitude of acceleration at the node on the 2nd floor slab of the building



*Figure 19: Magnitude of acceleration at the node on the 1st floor slab of the building*

Bednarz and Targosz (2011) suggested that the occupants tend to feel uncomfortable when the amplitude of the acceleration is above 0.005 times the gravitational constant. Another comfort criteria that was suggested by Murray (2003) proposed that the range of values where the occupants have an unpleasant feeling due to accelerated vibrations is between 0.5% and 5% of the gravitational constant value, depending on the frequency. Here, we observe in the acceleration graphs at different regions of the building structure that at the 1<sup>st</sup> floor, the maximum total acceleration value is 0.041 m/s<sup>2</sup> which is below the discomfort level while it is 0.052 m/s<sup>2</sup> at the 2<sup>nd</sup> floor slab which is above the discomfort level. The minimum limit above which discomfort is experienced is 0.049 m/s<sup>2</sup>. Therefore, there is concern that occupants may feel some discomfort. However, the amount is not so great that improved rail pads, ballast mats, or other mitigation techniques could not be used to reduce the vibration to acceptable levels. In taller buildings, the acceleration in upper floors may be higher due to swaying of the structure.

## **8 CONCLUSION**

In this research, in order to study the railroad system, an approach was used where the tools in finite element and multibody dynamics systems were applied in combination. The model includes a full representation of the track and substructure, with the geometry of the soil and a nearby building. This model was created for fulfilling the objective of evaluating the vibrations caused at different locations in the building structure transmitted through the soil due to a passing train.

A three-dimensional finite element model of a railway track consisting of the rail, sleepers, ballast, subballast, subgrade and a building structure with a foundation and wall was constructed in a finite

element package ANSYS. The ballast, subballast, subgrade and the concrete structure were modeled using 3D solid brick elements while the rail and sleepers were modeled using 3D beam elements. The rail pads and fasteners connecting the rail and the sleepers were modeled with spring-damper elements. A modal analysis was run for the entire model to extract the mode shapes and natural frequencies of the model along with its mass and stiffness matrices. This data was then used to extract the modal information for the rail nodes only using a nodal elimination technique. This method improves efficiency while allowing more complex details in the model. The rail-specific information was given to a multibody code to run the simulation of wheel-rail interaction. The multibody code computes the contact forces, modal displacements and acceleration for the rail system. The nodal data is reconstructed and fed back to ANSYS in the post-processing stage so that the results obtained can be visualized and studied easily. This nodal data was sorted and analyzed in MATLAB to plot graphs required to study the behavior of the moving train on the building structure and quantify the vibrations. Occupant discomfort was considered to study the vibrations at different levels of the building and checked for the given human comfort range. It was concluded that there is sufficient amount of vibration that would cause discomfort in some parts of the building structure, though not at all. It can be concluded that taller buildings can have higher vibrations in the higher levels than lower levels. This is due to the fact that the effect of bending and torsion due to structural flexibility can result in greater accelerations at higher levels of the building than as compared to levels which are close to the base of the building.

The model built in this research can provide results and help us study the behavior of moving trains over the substructure and its effects on adjacent building. There is further need to validate these results obtained from simulation and compared with the ones taken experimentally at different points on the building to measure the acceleration. Once validated, the model can be used to investigate various techniques for mitigating vibrations. Examining different rail pads, ballast materials, insulation for the building or other approaches to mitigating vibrations could help determine the most cost-effective techniques for mitigating vibrations in a given scenario.

## ACKNOWLEDGMENTS

This project was supported by the National University Rail (NURail) Center - a US DOT OST-R University Transportation Center.

## CITED LITERATURE

Bednarz, J. and Targosz, J. (2011). Finite elements method in analysis of vibrations wave propagation in the soil. *Journal of KONES Powertrain and transport*, 18(3).

Bian, X., Chen, Y. & Hu, T. (2008) Numerical simulation of high-speed train induced ground vibrations using 2.5D finite element approach. *Science China Series G-Physics, Mechanics, and Astronomy*. 51: 632.

Rosario Chamorro , Jose L.Escalona, Manuel Gonzalez (2011). An approach for modeling long flexible bodies with application to railroad dynamics. *Multibody Systems Dynamics* 26(2) 135-152

Chen, Y. H., and Y. H. Huang (2000). “Dynamic stiffness of infinite Timoshenko beam on viscoelastic foundation in moving co-ordinate.” *International Journal for Numerical Methods in Engineering* 48 (1): 1–18.

Connolly D.P., Galvín P., Olivier B., Romero A., Kouroussis G. (2019). A 2.5D time-frequency domain model for railway induced soil-building vibration due to railway defects. *Soil Dynamics and Earthquake Engineering* 120, 332-344.

El-Ghandour, A. I., Hamper, M. B., and Foster, C. D.: (2016) Coupled finite element and multibody system dynamics modeling of a three-dimensional railroad system, *Proceedings of the Institution of Mechanical Engineers, Part F: Journal of Rail and Rapid Transit*, Vol.230(I) 283-294,2016

El Ghandour, A. I. and Foster, C. D. (2019) Coupled Finite Element and Multibody Systems Dynamics Modeling to Investigate the Bridge Approach Problem. *Proceedings of the Institution of Mechanical Engineers, Part F: Journal of Rail and Rapid Transit*.

Galvín, P., François, S., Schevenels, M., Bongini, E., Degrande G., Lombaert, G. (2010)

A 2.5D coupled FE-BE model for the prediction of railway induced vibrations

*Soil Dynamics and Earthquake Engineering*, 30 (12) (2010), pp. 1500-1512

Galvín, P., Romero, A., Domínguez, J. (2010) Fully three-dimensional analysis of high-speed train-track-soil-structure dynamic interaction. *Journal of Sound and Vibration* 329, 5147–5163

Ghangale, D., Colaço A., Alves Costa, P., and Arcos R (2019) “A Methodology Based on Structural Finite Element Method-Boundary Element Method and Acoustic Boundary Element Method Models in 2.5D for the Prediction of Reradiated Noise in Railway-Induced Ground-Borne Vibration Problems” *Journal of Vibration and Acoustics* 141(3)

Hanson, C., Towers, D., Meister, L. High-speed ground transportation noise and vibration impact assessment. HMMH Report 293630-4, U.S. Department of Transportation, Federal Railroad Administration, Office of Railroad Development (October 2005)

Hanson, C., Towers, D., Meister, L: Transit noise and vibration impact assessment. Report FTA-VA-90-1003-06, U.S. Department of Transportation, Federal Transit Administration, Office of Planning and Environment (May 2006)

Kalker, J. (1990) *Three-Dimensional Elastic Bodies in Rolling Contact*. Kluwer Academic Publishers, Dordrecht, 1st edition.

Kouroussis G. and Verlinden O. (2015) Prediction of railway ground vibrations: Accuracy of a coupled lumped mass model for representing the track/soil interaction. *Soil Dynamics and Earthquake Engineering* 69, 220-226.

Kouroussis G., Vogiatzis K.E., Connolly D.P. (2017) A combined numerical/experimental prediction method for urban railway vibration. *Soil Dynamics and Earthquake Engineering*;97:377–86.

Krylov, V. V., A. R. Dawson, M. E. Heelis, and A. C. Collop. 2000. “Rail movement and ground waves caused by high-speed trains approaching track-soil critical velocities.” *Proceedings of the Institute of Mechanical Engineers Part F: Journal Rail Rapid Transit* 214 (2): 107–116.

Kumawat A.; Raychowdhury P., and Chandra S. (2019). “Frequency-Dependent Analytical Model for Ballasted Rail-Track Systems Subjected to Moving Load”. *International Journal of Geomechanics* 19 (4).

Kuo K.A., Papadopoulos M., Lombaert G., Degrande G. (2019). “The coupling loss of a building subject to railway induced vibrations: Numerical modelling and experimental measurements.”

*Journal of Sound and Vibration* 442, 459-481.

Kuo K.A., Verbraken H., Degrande G., Lombaert G. (2016). Hybrid predictions of railway induced ground vibration using a combination of experimental measurements and numerical modelling, *Journal of Sound and Vibration* 373 (2016) 263–284.

Kuppelwieser, H., Ziegler, A.: A tool for predicting vibration and structure-borne noise immissions caused by railways. *Journal of Sound and Vibration* 193, 261–267 (1996)

Lombaert G., Degrande G., François S., Thompson D.J. (2015) Ground-Borne Vibration due to Railway Traffic: A Review of Excitation Mechanisms, Prediction Methods and Mitigation Measures. In: Nielsen J. et al. (eds) *Noise and Vibration Mitigation for Rail Transportation Systems. Notes on Numerical Fluid Mechanics and Multidisciplinary Design*, vol 126. Springer, Berlin, Heidelberg

Masurekar, S. 3D FEM and MBS Coupled Model of Railroad System to Investigate the Vibrations in Surrounding Building Structures. Master’s thesis, University of Illinois at Chicago.

Meli, E. and Pugi, L. Preliminary development, simulation and validation of a weigh in motion system for railway vehicles, *Meccanica*, 48(10):2541–2565, 2013.

Murray, T.M., Allen, D.E., and Ungar, E.E (2003) Floor vibrations due to human activity, *American Institute of Steel Construction*.

O'Brien, J., Rizos, D. (2005) A 3D FEM-BEM methodology for simulation of high speed train induced vibrations. *Soil Dynamics and Earthquake Engineering* 25, 289–301

Recuero A.M., Escalona J.L., and Shabana, A.A.: Finite- element analysis of unsupported sleepers using three dimensional wheelrail contact formulation. *Proceedings of the Institute of Mechanical Engineers, Part K: Journal of Multi-body Dynamics*, 225 (2): 153-165, 2011.

Rücker W., and Auersch L. (2007). A user-friendly prediction tool for railway induced ground vibrations: emission - transmission - immision, in: 9th International Workshop on Railway Noise, Munich, Germany.

Shabana, A.A. : *Dynamics of Multibody systems*, Cambridge University press,2005

Shabana A. A., Zaazaa K. E., Sugiyama H.: *Railroad vehicle dynamics: A computational approach*. Boca Raton, FL, Taylor and Francis/CRC, 2007.

Shampine, L.F., and Gordon, M.K., 1975. *Computer Solution of Ordinary Differential Equations: The Initial Value Problem*. W.H. Freeman, San Francisco, USA.

Shih, J.Y., Thompson, D.J., Zervos, A. (2016) The effect of boundary conditions, model size and damping models in the finite element modelling of a moving load on a track/ground system, *Soil Dynamics and Earthquake Engineering* 89, 12-27

Toumi M., Chollet H., and Yin H. (2016) Finite element analysis of the frictional wheel-rail rolling contact using explicit and implicit methods, *An International Journal on the Science and Technology of Friction, Lubrication and Wear*, pages 157-166





**National University Rail Center - NURail**  
US DOT OST-R Tier 1 University Transportation Center

NURail Project ID: NURail2017-UIC-R16

## **Computational Analysis of Railroad Ballast Settlement**

By

Craig Foster  
Associate Professor  
Department of Civil and Materials Engineering  
University of Illinois at Chicago  
foster@uic.edu

29-08-2020

Grant Number: DTRT13-G-UTC52

## **DISCLAIMER**

Funding for this research was provided by the NURail Center, University of Illinois at Urbana - Champaign under Grant No. DTRT13-G-UTC52 of the U.S. Department of Transportation, Office of the Assistant Secretary for Research & Technology (OST-R), University Transportation Centers Program. The contents of this report reflect the views of the authors, who are responsible for the facts and the accuracy of the information presented herein. This document is disseminated under the sponsorship of the U.S. Department of Transportation's University Transportation Centers Program, in the interest of information exchange. The U.S. Government assumes no liability for the contents or use thereof.



## **TECHNICAL SUMMARY**

### **Title**

Computational Analysis of Railroad Ballast Settlement

### **Introduction**

Differential track settlement, especially near stiffness transitions, is a major issue in the rail industry. Settlement of ballast, and to a lesser extent subballast and subgrade, can degrade ride quality, increase wear on track and train components, and, if left unchecked, lead to derailment. A number of attempts, from empirical to discrete element models, have been made to attempt to predict settlement. In this research we use a coupled finite element and multibody dynamics model to predict settlement, incorporating an advanced viscoplastic model for the track substructure.

### **Approach and Methodology**

In this report, finite element (FE) structural dynamics algorithms are used to develop detailed railroad track substructure models to analyze the differential settlement in the ballast due to dynamic cyclic loading conditions. A cap plasticity material model is used in order to capture the geotechnical behavior of the ballast. The cap plasticity model includes enhancements to the Sandia GeoModel, such as improved computational tractability, robustness and domain of applicability. The material properties needed for the plasticity GeoModel are characterized with the help of several experimental triaxial compression tests on rail ballast. The finite element model is fed into a multibody dynamics code to determine wheel-rail contact forces, which are then used to find the permanent displacements in the substructure.

### **Findings**

Reasonable agreement is obtained compared discrete element models. The model is reasonably computationally efficient compared to the most physically motivated models.

### **Conclusions**

The proposed method can be employed to predict settlement of tracks, along with examining mitigation techniques. More validation is needed, and further fitting is required for the viscous properties before the model can be used in a quantitatively predictive fashion.

## **Recommendations**

Continued validation and comparison with instrumented sites are needed.

## **Publications**

Motamedi, M. H. and Foster, C. D.: An improved implicit numerical integration of a non-associated, three-invariant cap plasticity model with mixed isotropic-kinematic hardening for geomaterials. *International Journal for Numerical and Analytical Methods in Geomechanics*, 39(17):1853–1883, 2015.

C.D. Foster and S. Kulkarni. “Coupled Multibody and Finite Element Modelling of Track Settlement.” 16<sup>th</sup> International Conference of the International Association for Computer Methods and Advances in Geomechanics, May 5-8, Turin, Italy.

## **Primary Contact**

### **Principal Investigator**

Craig Foster  
Associate Professor  
Department of Civil and Materials Engineering  
University of Illinois at Chicago  
(312) 996-8086  
foster@uic.edu

### **Other Faculty and Students Involved**

Erol Tutumluer  
Professor  
Department of Civil Environmental Engineering  
University of Illinois at Urbana-Champaign  
(217) 333-8637  
tutumlue@illinois.edu

Shubhankar Kulkarni  
Graduate Research Assistant  
Department of Mechanical and Industrial Engineering  
University of Illinois at Chicago

(312) 996-0438  
skulka22@uic.edu

Mohammad Hosein Motamedi  
Graduate Research Assistant  
Department of Civil and Materials Engineering  
University of Illinois at Chicago  
(312) 996-0438  
mmotam2@uic.edu

Ahmed El-Ghandour  
Graduate Research Assistant  
Department of Civil and Materials Engineering  
University of Illinois at Chicago  
(312) 996-0438  
aelgha2@uic.edu

Yu Qian  
Research Staff  
Department of Civil Environmental Engineering  
University of Illinois at Urbana-Champaign  
Yuqian1@illinois.edu

**NURail Center**  
217-244-4999  
[nurail@illinois.edu](mailto:nurail@illinois.edu)  
<http://www.nurailcenter.org/>

## ABSTRACT

In this paper, finite element (FE) structural dynamics algorithms are used along with multibody systems (MBS) techniques to develop detailed railroad track substructure models to analyze the differential settlement in the ballast due to dynamic cyclic loading conditions. A cap plasticity material model is used in order to capture the geotechnical behavior of the ballast. The cap plasticity model includes enhancements to the Sandia GeoModel, such as improved computational tractability, robustness and domain of applicability. The material properties needed for the plasticity GeoModel are characterized with the help of several experimental triaxial compression tests on rail ballast. The ballast is divided into elastic and plastic regions to represent areas where the railway track is more prone to differential settlement, such as the ends of tunnels or passages over culverts. The rails are modeled using the absolute nodal coordinate formulation-based (ANCF) gradient-deficient beam elements, allowing seamless integration of beams with nonlinear structural dynamics algorithms. The solver to numerically integrate of the second order differential equations of motion is implemented in an in-house code. MBS algorithms are used to extract wheel-rail contact forces. Numerical results are presented and analyzed in the presence and absence of inelasticity considerations for the ballast.

**Keywords:** Plasticity; ballast modeling; differential settlement; railroad vehicle dynamics; multibody dynamics, finite elements

## 1. INTRODUCTION

In the past few decades, the development of high-speed railways has become crucial to the transportation infrastructure in many countries around the world. Some high-speed railways still run on ballasted track (Tutumluer et al., 2013), and therefore a large amount of research effort has been devoted towards better understanding, and optimizing the design and maintenance procedures of the ballasted rail substructures. A typical railroad track substructure constitutes a top layer of ballast, an intermediate layer of subballast, followed by a bottom layer of subgrade, which often undergoes some form of soil improvement. The ballast layer serves several important functions such as providing supportive resistance to multi-directional loads from the trains, providing shock absorbing characteristics for the substructure, distributing the sleeper loads uniformly throughout the substructure to prevent subgrade from experiencing high stresses, retarding the vegetation growth rate beneath the track and facilitating easier maintenance for the substructure. The rail track undergoes significant permanent settlement after being subjected to numerous loading cycles. The major contribution towards the settlement comes from the ballast layer (Dahlberg, 2001). The track settlement can cause decreased ride quality, increased wear, and in some cases it may even lead to derailment (Li et al., 2014). This investigation is focused on computational modeling of the rail ballast settlement using the finite element (FE) structural dynamics algorithms, where the ballast will be characterized by a cap plasticity model. FE method is coupled with MBS techniques to extract wheel-rail contact forces. In this section, a brief literature survey of different computational and analytical settlement models is provided. The specific contributions of this study and the organization of the paper are also discussed.

### 1.1 Background

The settlement of ballast has been an extensive topic of research as it contributes significantly to the cost of track maintenance. The ballast is usually made of non-cohesive and granular materials like uniformly crushed granite, quartzite, basalt or other rocks with similar material properties. The granular nature of the ballast material characterizes the track settlement usually into two phases (Dahlberg, 2001). The first phase of settlement is relatively fast and is caused by adjustment of granular particles to fill the gaps in the ballast, resulting into a denser structure. In the relatively slower second phase of settlement, in addition to the continued compaction process, there are several factors which contribute to the settlement. The granular particles further break down into smaller pieces, and are subjected to abrasive wear which gradually adds to the settlement. In addition to these factors, the inelastic recovery of the ballast in the second phase continues due to relative micro-scale slippage between the particles, and displacement of the particles away from the rails as the sleepers penetrate into the ballast. Representing this complex mechanism of plastic settlement with a numerical model is a challenging task, and it has been dealt with in the literature using empirical and analytical models, the discrete element method (DEM) and the finite element method (FEM).

Most of the analytical and empirical models present in the literature consider settlement as a function of number of loading cycles and the magnitude of the wheel-rail contact load (Dahlberg, 2001; Ford, 1995; Indraratna et al., 2009, Mauer, 1995; Sato, 1997). In such models, there is very little scope to

accommodate high-fidelity ballast material characterization in order to accurately predict the plastic settlement. Furthermore, consideration of detailed geometry to assess high-stress areas and sleeper-ballast contact pressure is not easy using these analytical models. As observed by Dahlberg (2001), different analytical settlement models in the literature usually do not lead to the same solution as it is not straightforward to characterize empirical constants for different ballast materials and geometries.

A more physically motivated approach used in the computational analysis of railroad ballast is the DEM, a discontinuum-based numerical analysis approach (Nishiura et al., 2017; Tutumluer et al., 2013). The DEM considers each particle in the discrete material as a separate element. The interaction between these rigid elements, particularly interface contact forces and energy dissipation, are computed at each numerical time-step. The DEM is capable of modeling complex particle shapes such as granular ballast, and the granular nature of the ballast makes DEM one of the most appropriate approaches to evaluate track settlement. However, such shapes require sophisticated contact detection algorithms. Furthermore, a large number of particles can result into a numerical model having a large number of degrees of freedom, making this approach computationally expensive. Tutumluer et al. (2007) studied the effect of load magnitude and load application frequency on the ballast settlement and found out that lower loading frequencies result into higher plastic settlement. Huang and Tutumluer (2011) used an image-aided DEM approach to simulate and validate coal-dust-fouled-track settlement performance and showed that fouled ballast settles more rapidly than clean ballast, and can lead to the creation of ‘hanging sleepers’. Indraratna et al. (2009) investigated the effect of frequency of loading on ballast fouling using 2D DEM simulations and laboratory experiments. To represent the ballast aggregate, fifteen particles of different shapes were generated in the form of cluster of bonded circular particles using 2D image projection methods. Lu and McDowell (2010) modeled the triaxial samples of ballast by grouping ten spherical particles to form tetrahedral particle shapes along with eight smaller particles to represent asperities. Mahmoud et al. (2016) used two different methods to capture ballast particle shapes and studied the shapes’ effects on DEM simulation results. They concluded that hexagonal assembly method to represent ballast particles yielded the most realistic results. Some of these approaches, especially the ones representing ballast particles using clumps of spheres, keep computational costs reasonable and capture particle breakage. However, these approaches may not be able to represent the macroscopic interactions between angular particles correctly (Tutumluer et al., 2018).

Another numerical technique used in the analysis of ballast settlement is the finite element method (FEM). The finite element (FE) approach to evaluate ballast behavior offers high fidelity in terms of modeling nonlinear material behavior and capturing detailed geometry at a reasonable computational cost. Dahlberg (2001) created a simplified FE model using linear and nonlinear spring-like elements to represent stiffness properties of different components in the railway substructure. Lundqvist and Dahlberg (2005) studied the effect of hanging sleepers on track response and sleeper-ballast contact forces for different prescribed values of gap between the sleepers and the ballast. The entire rail track structure was modeled using the FEM. Similar simplified FE, multibody and semi-analytical models of the railway track structure can be found in the literature (Huang et al., 2010; Kalker 1996; Recuero et



al., 2011). El-Ghandour et al. (2016), El-Ghandour and Foster (2019)) coupled the FEM with nonlinear multibody dynamics algorithms to evaluate the elastic dynamic response of the rail substructure. The rail track structure was modeled using the FE floating frame of reference formulation in multibody dynamics framework to accurately account for the coupled wheel-rail contact forces with the substructure deformations. Kaewunruen and Mirza (2017) investigated the bridge-approach problem using a hybrid FEM-DEM model. The ballast was modeled using the DEM whereas the other components in the rail track structure were modeled using the FEM. A few investigations in the literature (Indraratna and Nimbalkar, 2013; Jiang and Nimbalkar, 2019) represented a cross-section of railway substructure using 2D plane-strain FE model. The plastic behavior of the ballast was modeled using the hardening soil model (Schanz et al., 1999). The current investigation uses FE analysis to evaluate the ballast behavior under cyclic loading using a cap plasticity soil model. Specific technical contributions of this investigation are given below.

## **1.2 Scope of this Investigation**

The primary objective of this study is to establish a novel FE dynamics-based framework to model and analyze the rail track structure and the elasto-viscoplastic behavior of the ballast under cyclic dynamic loading conditions. The FEM coupled with MBS techniques offers a new approach to simulate the geotechnical interactions in the railroad substructure at a reasonable computational cost and efficiency compared to the DEM approach. The FE and MBS codes are executed separately. The MBS code is run first with an equivalent rigid track model to extract the wheel-rail contact forces. In the second step, the FE code is executed in the time domain with a detailed rail substructure geometry, and the time-dependent wheel-rail contact forces are applied on the flexible rails in the FE model to extract the model response. This approach offers advantages of both MBS and FE methodologies. Furthermore, the user has more control over choosing and characterizing the material properties than the simplified empirical ballast settlement models. Specifically, the main contributions of this paper can be summarized as follows:

- (1) A comprehensive FE model of rail track structure is built to analyze the effect of train cyclic loading on the railway substructure, particularly the inelastic settlement of the ballast in the areas of stiffness transitions. The three-dimensional geometry of the structure is meshed using trilinear eight-node brick elements and the rails are modeled using two-node cubic beam elements. The time-dependent force boundary conditions are extracted from an MBS code.
- (2) Areas of non-uniform settlement are central to this investigation. In order to represent such a transition, the ballast is divided into elastic and plastic parts. The plastic part, which represents the granular ballast material, is modeled as a continuum with a cap plasticity model previously proposed by the authors (Motamedi and Foster, 2015). This cap plasticity model includes enhancements to the Sandia GeoModel, such as improved tensile behavior, computational tractability, robustness and domain of applicability.

- (3) The material properties for the aforementioned inelasticity model are derived methodically from triaxial experimental test data to accurately represent the granular ballast material.
- (4) MBS dynamics techniques are coupled with FE algorithms to extract the wheel-rail contact forces. These forces act as time-dependent boundary conditions in the FE code, where the detailed railroad substructure model is executed in the time domain.
- (5) The entire FE solver is implemented using an object-oriented code in MATLAB. Fully implicit Newmark- $\beta$  numerical integration scheme with adaptive time-stepping is used to time-march the equations of motion.
- (6) Numerical results are presented to analyze the geotechnical behavior of the ballast and the rest of the substructure with and without plasticity considerations.
- (7) The effect of different wheel-rail contact load magnitudes and train velocities on the ballast settlement is explored through multiple simulations.

### 1.3 Organization of the Paper

Section 2 of the paper elaborates the elasto-viscoplastic material model employed to represent the ballast. The material properties for the inelastic material model are systematically derived in Section 3. In Section 4, the FE model of the railroad track structure is described in depth along with the implementation details of the solver. In the following section, Section 5, the wheel-rail contact formulation used in the MBS code is explained. The numerical results from different simulations are reported and discussed in Section 6. The effects of varying load magnitude and train velocity on ballast settlement are studied, with a focus on areas of non-uniform differential settlement. In Section 7, summary and conclusions are presented.

## 2. PLASTICITY MATERIAL MODEL

The inelastic deformation is accounted for using a version of the Sandia GeoModel (Fossum and Brannon, 2004, Foster et al. 2005). The model was updated in Motamedi and Foster (2015), to better account for tensile yielding as well as improve the numerical robustness and efficiency. The model is summarized here, but the reader is referred to the above references for details of the implementation.

The failure surface is composed of a shear surface, plus multiplicative caps both in tension and compression. The shear surface, originally proposed by Simo and Ju (1987), is nonlinear with the form

$$F_f = A - C \exp(BI_1) - \theta I_1 \quad (1)$$

where,  $I_1$  is the first invariant of the stress and  $A$ ,  $B$ ,  $C$  and  $\theta$  are material constants. The shear yield surface is offset from the failure surface by a parameter  $N$ . This yield surface is multiplied by a tension and compression cap functions, which can be combined and written as

$$F_c(I_1, \kappa, T) = 1 - H(\kappa - I_1) \left( \frac{I_1 - \kappa}{X(\kappa) - \kappa} \right)^2 - H(I_1 - I_1^T) \left( \frac{I_1 - I_1^T}{T - I_1^T} \right)^2 \quad (2)$$

Here,  $H$  is the Heaviside function,  $\kappa$  and  $I_1^T$  mark the onset of the compression and tension caps, respectively, and,  $X$  and  $T$  are the limits of  $I_1$  the hydrostatic compression and tension strength. The parameter  $X$  evolves with  $\kappa$

$$X = \kappa - RF_f(\kappa) \quad (3)$$

The entire yield function, then, can be written as

$$f = \Gamma(\beta^\xi) \sqrt{J_2^\xi} - \sqrt{F_c}(F_f - N) \quad (4)$$

and is shown in Figure 5. In Eq. 4,  $J_2^\xi$  is the opposite of the second invariant of the deviatoric component of the relative stress  $\xi = dev(\boldsymbol{\sigma}) - \mathbf{a}$ . The function  $\Gamma$  is a third-invariant modifying function. In the work, we use the Gudehus function

$$\Gamma(\beta^\xi) = \frac{1}{2} \left[ 1 + \sin(3\beta^\xi) + \frac{1}{\psi} (1 - \sin(3\beta^\xi)) \right] \quad (5)$$

where  $\beta^\xi = \sqrt{3} J_3^\xi / (2(J_2^\xi)^{3/2})$  is the Lode angle of the relative stress tensor and  $\psi$  is the ratio of triaxial extension to compression strength. The plastic potential has a similar form, but with modified parameters to prevent to overprediction of dilation.

There are two hardening variables, the cap parameter  $\kappa$  and the deviatoric back stress  $\psi$  the back stress evolves as  $\dot{\mathbf{a}} = c^\alpha G^\alpha dev(\dot{\boldsymbol{\epsilon}}^p)$ , where  $c^\alpha$  is a material constant, and,

$$G^\alpha = 1 - \frac{\sqrt{J_2^\alpha}}{N} \quad (6)$$

where,  $J_2^\alpha = \frac{1}{2} \mathbf{a} : \mathbf{a}$ . The cap parameter evolves with the volumetric plastic strain and can be written as

$$\dot{\kappa} = \dot{\epsilon}_v^p \left/ \left( \frac{\partial \epsilon_v^p}{\partial X} \frac{\partial X}{\partial \kappa} \right) \right. \quad (7)$$

Here,  $\varepsilon_v^p$  is the plastic volumetric strain, which is assumed to be a function of  $X$  given by

$$\varepsilon_v^p = W \left( \exp \left[ D_1 (X(\kappa) - X_0) - D_2 (X(\kappa) - X_0)^2 \right] - 1 \right) \quad (8)$$

for given material parameters  $W$ ,  $D_1$  and  $D_2$ . Often the last parameter is taken to be zero.

### 3. MATERIAL PROPERTIES AND FITTING PROCEDURE FOR THE GEOMODEL

This section describes the fitting procedure to obtain material properties for the plasticity GeoModel. For more details and motivation of the material parameterization, the reader is referred to Fossum and Brannon (2004) and Motamedi (2016). While many of the material parameters have a clear physical meaning and can be easily derived, others, in particular the hardening parameters, do not have an easy physical interpretation.

#### 3.1 Linear Elastic Parameters

Young's modulus can be derived from the initial linear part of the stress-strain response of the uniaxial or triaxial compression tests. Similarly, Poisson's ratio can also be easily determined from linear strain response of uniaxial stress state,  $\nu = -\varepsilon_{axial} / \varepsilon_{lateral}$ . However, in this case, the volumetric strain data, from which the lateral strain can be readily recovered, was not available. Estimates for the Poisson's ratio were taken from the literature.

#### 3.2 Shear Failure Envelope Parameters

In order to derive the material parameters for the shear failure surface, a set of triaxial compression (TXC) tests are required. Figure 1 represents the shear failure surface along with a series of triaxial loading tests depicted in meridional stress space ( $\sqrt{J_2}$  versus  $I_1$ ). Figure 2 shows the peak stress values for three sets of a triaxial test for the ballast material with confining pressure values of  $P = 68$  KPa, 103 KPa, and 138 KPa. A linear fit is used to generate the required data. In order to fit an exponential curve of the form shown in Fig. 1 with the high degree of accuracy, more peak data pairs, particularly at high confining pressures, are required. Therefore, the parameters  $A$  and  $\theta$  were derived from the linear portion of the curve. The parameters  $B$  and  $C$  are taken to be zero.

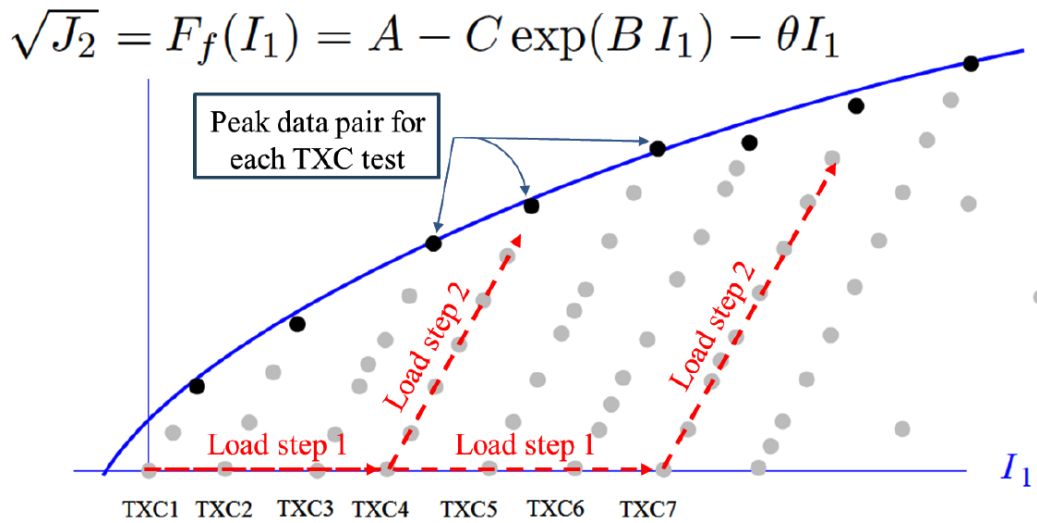


**Figure 1.** Shear failure surface using triaxial compression (TxC) tests

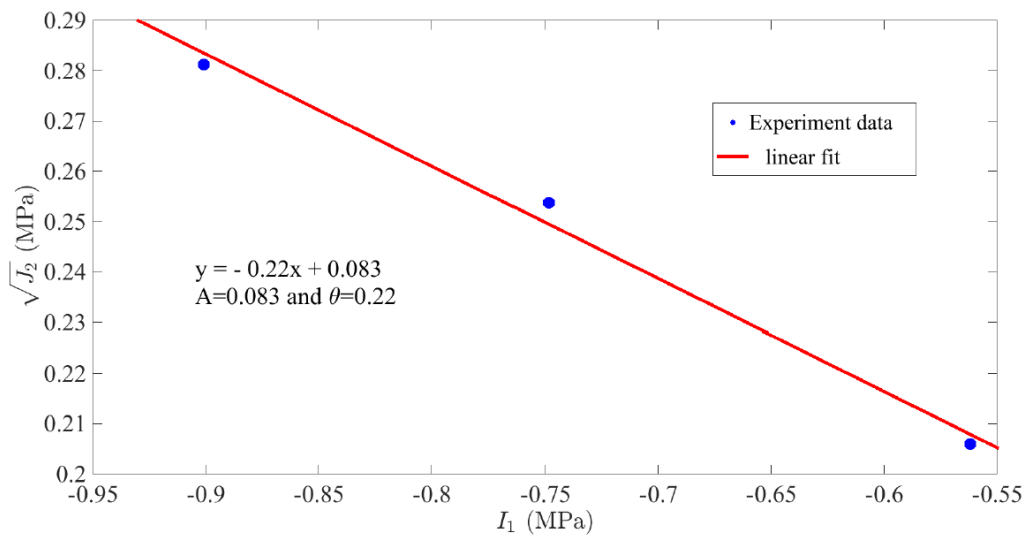


**Figure 2.** Shear failure surface parameters for the plastic ballast

### 3.3 Kinematic Hardening Parameters

Using the triaxial compression test allows us to derive two additional parameters incorporated in shearing-induced kinematic hardening of the model. The two parameters of interest are the yield failure surface offset parameter,  $N$ , and the scalar decay parameter,  $c^\alpha$ . The parameter  $N$  is the maximum kinematic translation that can occur before reaching the failure limit surface (Sutley, 2009). The parameter  $c^\alpha$  assigns the rate at which the initial yield surface translates to the failure envelope of

the surface. Figure 3 illustrates the effect of the offset parameter,  $N$ . The plot shows a simulated triaxial test. The offset parameter can be increased to allow for nearly instantaneous yielding which is often observed in soils.

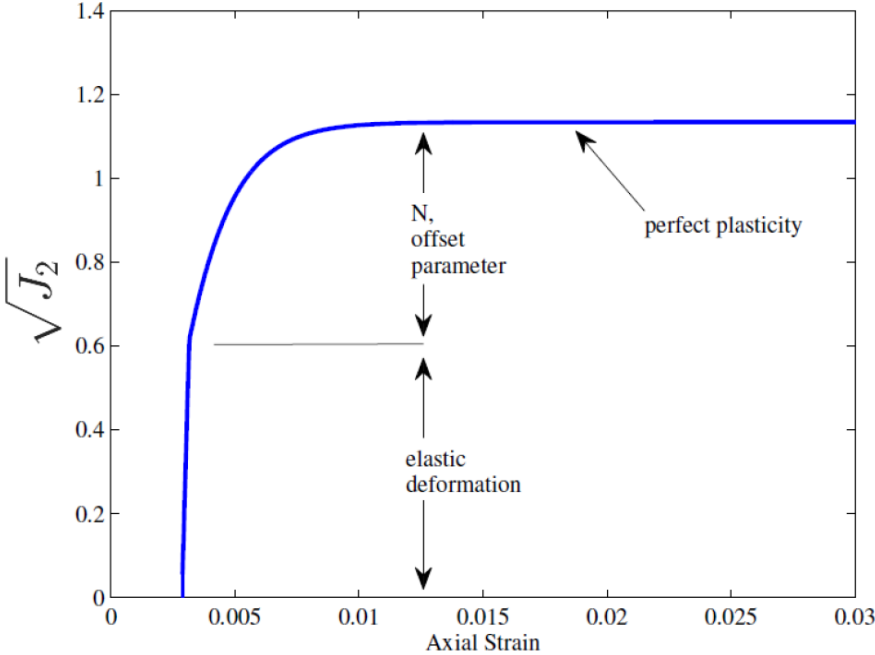


**Figure 3.** Illustration of the offset parameter – N

Figure 4 demonstrates the influence of the kinematic hardening parameter  $c^\alpha$ . As  $c^\alpha$  increases, the initial yield surface approaches the failure surface more sharply (Sutley, 2009). Considering different values of  $c^\alpha$  enables us to fit the nonlinear yield response of the experimental data more accurately. As a result, for the rail ballast material, a trial and error method was used to capture acceptable values for these two parameters in accordance with triaxial data plotted in Fig. 6.

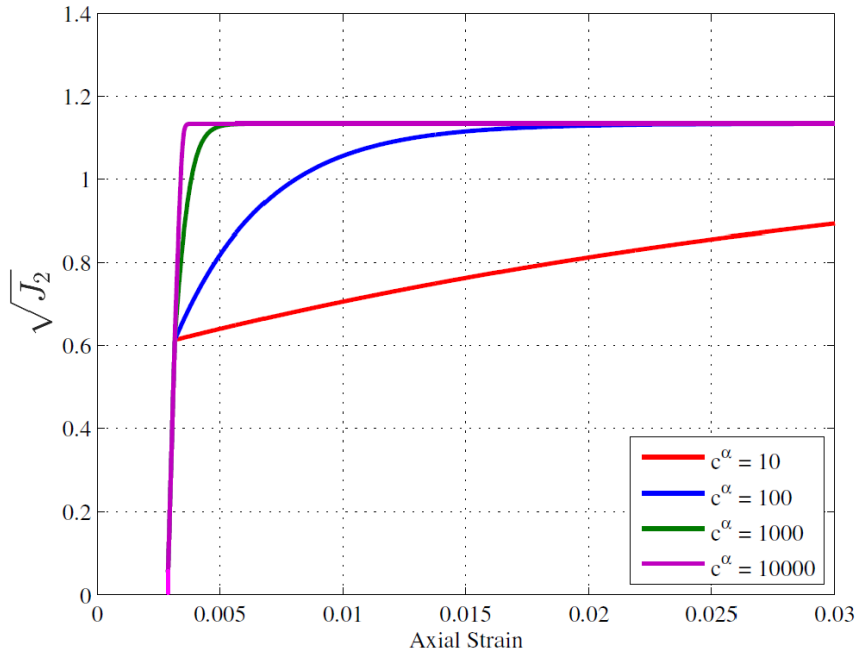


**Figure 4.** The effect of the kinematic hardening parameter -

### 3.4 Material Parameterization of the Cap Plasticity Model for the Ballast Material

The experimental data for ballast material is utilized to fit the material parameters of the cap plasticity model. This data is obtained under triaxial loading tests with three levels of confining pressure - 68 KPa, 103 KPa, and 138 KPa. The material properties listed in Table 1 were fit using this data. A two-dimensional representation of the shear failure surface, initial yield surface, and conjugated plastic potential surface are illustrated in Fig. 5. In addition, Fig. 6 compares the low rate triaxial loading test data with corresponding numerical simulations.

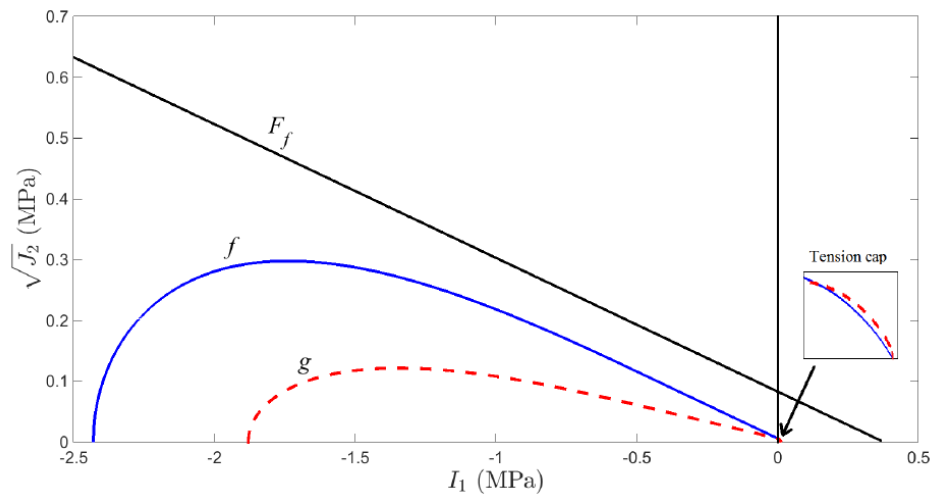


**Figure 5.** Shear failure surface, initial yield and plastic potential surface in meridional stress space (versus )

**Table 1.** Material properties for the ballast cap plasticity material

Parameter	Value
Young's modulus ( $E$ )	85 (MPa)
Poisson's ratio ( $\nu$ )	0.3 (-)
Isotropic tensile strength ( $T$ )	0.05 (MPa)
Tension cap parameter ( $I_1^T$ )	0.0 (MPa)
Compression cap parameter ( $K_0$ )	-0.5 (MPa)
Shear yield surface parameter ( $A$ )	0.08 (MPa)
Shear yield surface parameter ( $B, L$ )	0.0 (1/MPa)
Shear yield surface parameter ( $C$ )	0.0 (MPa)
Shear yield surface parameter ( $\theta$ )	0.22 (rad)
Shear yield surface parameter ( $\phi$ )	0.11 (rad)
Aspect ratios ( $R, Q$ )	10 (-)
Kinematic hardening parameter ( $c^\alpha$ )	1E5 (MPa)
Kinematic hardening parameter ( $N$ )	0.075 (MPa)
Stress triaxiality parameter ( $\psi$ )	1 (-)

### 3.5 Rate Dependence

The viscoplastic parameter is fit from triaxial tests at different strain rates. As there is no ready formula to calculate directly, this parameter is fit through a trial and error procedure after the yield



surface and hardening parameters are fit from the slow tests. Similarly, elastic damping constants can be fit from the elastic portion of the curve. It is worth noting, however, the even high-rate triaxial tests have lower strain rates than soil vibrations, so these parameters are estimates.

#### **4. RAILROAD TRACK STRUCTURE FE MODEL**

This section describes the FE railroad substructure model and presents the nonlinear dynamic equations that govern the behavior of the system. The ordinary differential equations (ODEs) of motion are formulated and solved using an in-house object-oriented MATLAB code. The implementation details of absolute nodal coordinate formulation-based (ANCF) beam element used for modeling the rails are provided in this section as well. The wheel-rail contact forces extracted from the MBS code act as the time-dependent boundary conditions in the FE model.

##### **4.1 Geometry and Meshing**

Figure 7 shows a schematic of the railway track numerical model created in this investigation. The track superstructure includes rails, rail pads and sleepers. The rails are meshed using ANCF gradient-deficient Euler-Bernoulli beam elements. The connecting pads between rails and sleepers are represented by linear one-dimensional spring-damper elements. The rails are oriented along the global X-axis, whereas the rail pads are placed vertically along the global Z-axis. The rails are total 10.8 m in length, and they extend beyond the substructure mesh on both sides in order to mitigate the boundary effects. The substructure body is located in the central span of the rails with a dimension of 3.6 m along the direction of the rails. The parts of the rails which extend before and after the substructure geometry are connected to the ground through fastener spring-dampers. The sleepers are placed equidistantly with a distance of 0.6 m between them.

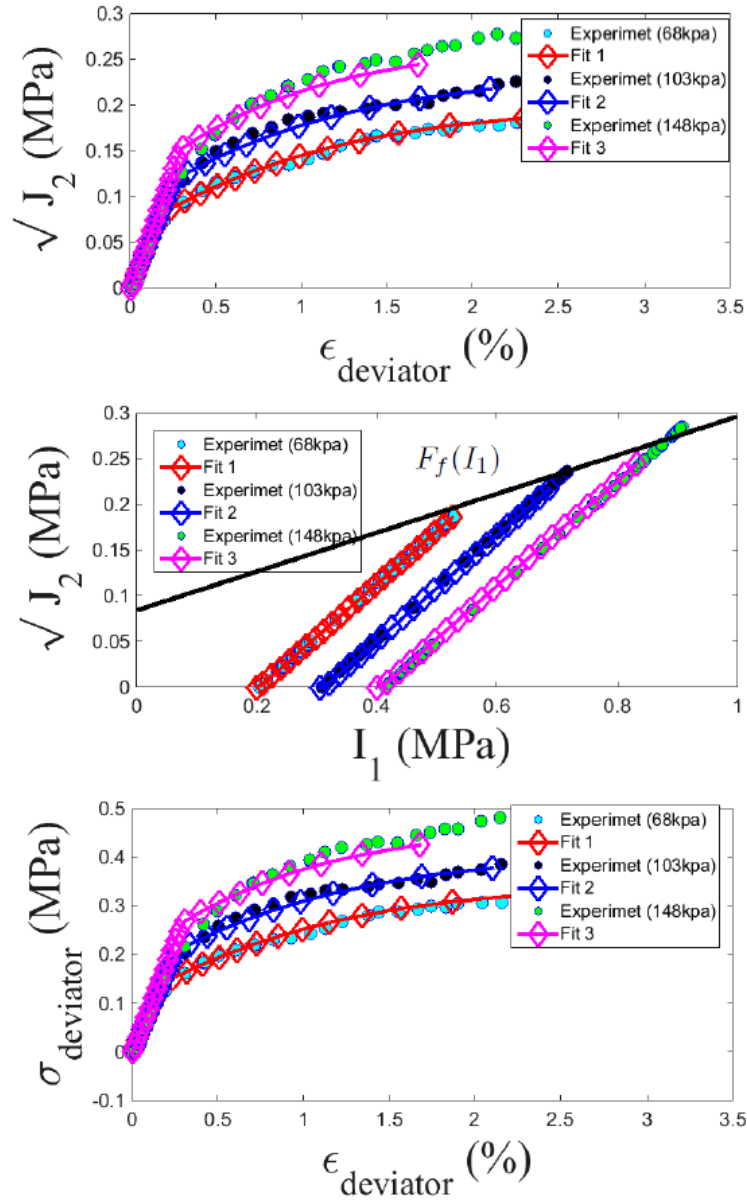


**Figure 6.** Experimental data and corresponding numerical simulations for triaxial loading tests of ballast material

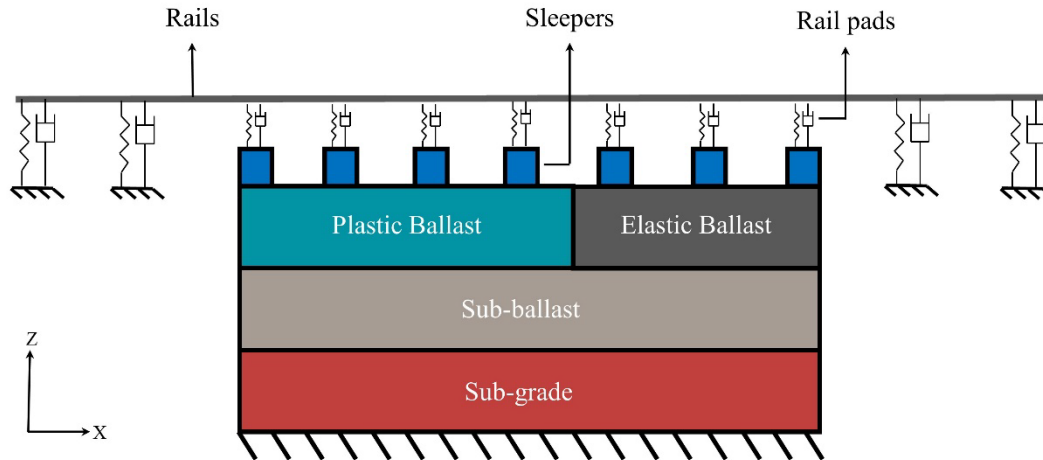


**Figure 7.** Railway track numerical model

Detailed substructure geometric dimensions and mesh are shown in Fig. 8. The substructure consists of the ballast, subballast and subgrade. Halfway along the track, the ballast is replaced by an elastic concrete slab, representing a stiffness transition analogous to passages over culverts or end of tunnels. The concrete slab does not undergo large permanent settlement as compared to the granular ballast, and this differential settlement severely affects the railroad vehicle dynamics. The entire substructure geometry is meshed with trilinear eight-node three-dimensional isoparametric brick elements. The number of brick elements and beams used in the FE model are 2564 and 72, respectively, which constitutes to 8972 total degrees of freedom.

#### 4.2 ANCF Beam Elements for Rails

The absolute nodal coordinate formulation (ANCF) is a non-incremental FE formulation which is often used in multibody systems dynamics to describe flexible bodies undergoing large arbitrary reference motions and large deformations (Daocharoenporn et al., 2019; Grossi and Shabana, 2018; Kulkarni et al., 2017; Patel et al., 2016). The ANCF beams are classified as isoparametric elements as opposed to conventional FE beams which use incremental rotations as nodal coordinates. The ANCF beam elements use global positions and position vector gradients as nodal coordinates (Kulkarni and Shabana, 2019).

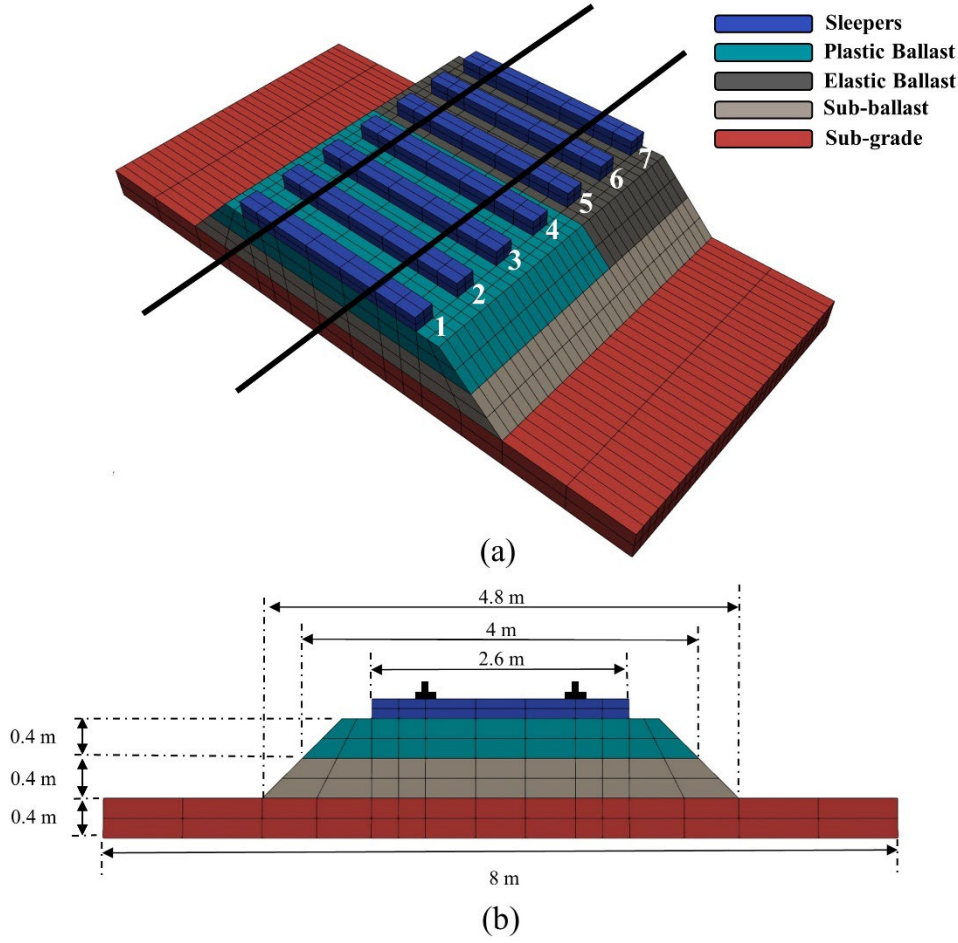


**Figure 8.** Railroad track substructure geometry and mesh

The ANCF gradient-deficient cable element is used in this investigation to model the rails. ANCF cable elements allow representing accurately the geometric nonlinearities and do not suffer from the locking problems encountered with other conventional and fully-parameterized ANCF finite elements (Gerstmayr and Shabana, 2006). The cable elements can also capture the stretch and bending deformation modes, and therefore, they are well suited for the problem considered in this investigation. In general, the global position of an arbitrary point on an ANCF element is defined as

$\mathbf{r}(\mathbf{x}, t) = \mathbf{S}(\mathbf{x})\mathbf{e}(t)$ , where  $\mathbf{x} = [x \ y \ z]^T$  is the vector of the element spatial coordinates,  $\mathbf{S} = \mathbf{S}(\mathbf{x})$  is the space-dependent shape function matrix, and  $\mathbf{e} = \mathbf{e}(t)$  is the vector of the time-dependent element nodal coordinates. For an ANCF cable element,  $\mathbf{S} = \mathbf{S}(x)$ , and the vector of time-dependent nodal coordinates is defined for node  $k$  as  $\mathbf{e}^k = \left[ (\mathbf{r}^k)^T \ (\mathbf{r}_x^k)^T \right]^T$ ,  $k = 1, 2$ . The space-dependent matrix of shape functions is  $\mathbf{S} = [s_1\mathbf{I} \ s_2\mathbf{I} \ s_3\mathbf{I} \ s_4\mathbf{I}]$ , where

$$\left. \begin{aligned} s_1 &= 1 - 3\xi^2 + 2\xi^3, & s_2 &= L(\xi - 2\xi^2 + \xi^3), \\ s_3 &= 3\xi^2 - 2\xi^3, & s_4 &= L(-\xi^2 + \xi^3) \end{aligned} \right\} \quad (9)$$

In this equation,  $L$  is the length of the element, and  $\xi = x/L$ . The kinematics of this element are shown in Fig. 9. This ANCF cable element has a constant mass matrix  $\mathbf{M}_e = \int_0^L \rho_e A_e \mathbf{S}^T \mathbf{S} dx$ , where,  $\rho_e$  is the density of the material used for the cable, and  $A_e$  is the cross-sectional area. The elastic force formulation has been simplified for the purposes of this investigation as rigid-body motion and large deformation are not encountered while modeling rails. The small-deformation elastic force formulation and the expression for tangent stiffness matrix can be found in Hamed et al. (2015).

There are several advantages of using the ANCF cable element in this investigation. This element is directly compatible with spatial structural dynamics algorithms without the need for using incremental procedures and has a constant mass matrix. A minor noteworthy aspect of this element in the context of solver implementation is that absolute states are integrated as opposed to integrating displacements for the classical brick elements. This element performs very efficiently when being used with the simplified elastic force formulation.

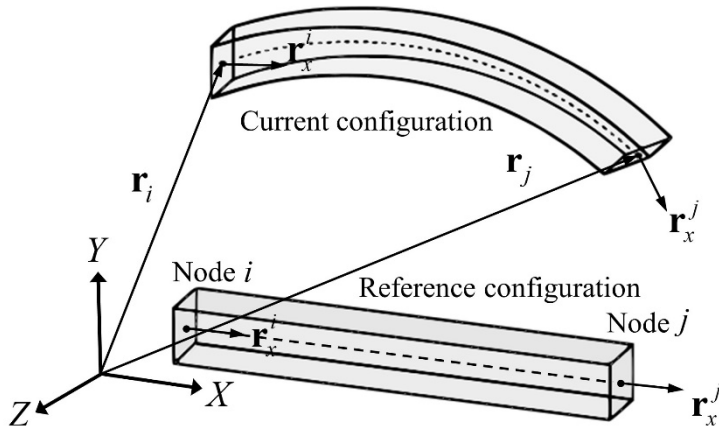


**Figure 9.** ANCF cable element

### 4.3 Material Properties and Boundary Conditions

In the FE model of the railway track substructure, other than the plastic part of the ballast, all other components are modeled with linear elastic materials. Table 2 provides the material properties for all of the elastic components.

The rails, which are modeled with ANCF cable elements, are constrained in the lateral and longitudinal directions at both ends, and all other rail nodes are constrained in the lateral direction only. All nodes

belonging to the bottom face of the subgrade are fully constrained in all three spatial directions. The nodes on all four side-faces of the substructure are constrained along the direction perpendicular to the face containing the node. The spring elements which belong to the rail spans that extend before and after the substructure, are constrained at the bottom node as shown in Fig. 7.

#### 4.4 Equations of Motion

The second order nonlinear differential equations of motion are given by,

$$\left. \begin{aligned} \mathbf{M}\ddot{\mathbf{u}} + \mathbf{r}(\mathbf{u}, \dot{\mathbf{u}}) &= \mathbf{f}(t) \\ \mathbf{u}(t_0) = \mathbf{u}_0, \dot{\mathbf{u}}(t_0) &= \dot{\mathbf{u}}_0 \end{aligned} \right\} \quad (10)$$

**Table 2.** Material properties of linear elastic components in the FE model

Component	Parameter	Value
Rails	Length	10.8 (m)
	Gauge length	1.5113 (m)
	Young's modulus	2.1E11 (Pa)
	Density	7700 (kg/m <sup>3</sup> )
	Poisson's ratio	0.3 (-)
	Cross-section area	64.5E-4 (m <sup>2</sup> )
	Second moment of inertia ( $I_{yy}$ )	2.01E-5 (m <sup>4</sup> )
	Second moment of inertia ( $I_{zz}$ )	3.26E-6 (m <sup>4</sup> )
Rail Pads (Fasteners)	Stiffness	2.65E8 (Pa)
	Damping coefficient	4.6E4 (Ns/m)
Sleepers	Young's modulus	6.4E10 (Pa)
	Density	2750 (kg/m <sup>3</sup> )
	Poisson's ratio	0.25 (-)
Elastic Ballast (Concrete Slab)	Young's modulus	3.2E10 (Pa)
	Density	2750 (kg/m <sup>3</sup> )
	Poisson's ratio	0.25 (-)

Sub-ballast	Young's modulus	2.0E8 (Pa)
	Density	1850 (kg/m <sup>3</sup> )
	Poisson's ratio	0.35 (-)
Sub-grade	Young's modulus	2.0E8 (Pa)
	Density	1850 (kg/m <sup>3</sup> )
	Poisson's ratio	0.3 (-)

Where  $\mathbf{M}$  is the constant mass matrix,  $\mathbf{f}$  is the vector of generalized elastic forces. The generalized time-dependent external force vector is denoted by  $\mathbf{f}(t)$ . In a nonlinear problem, such as the one being solved in this investigation, the stiffness and damping matrices become explicit functions of the independent states,  $\mathbf{u}$  and  $\dot{\mathbf{u}}$ . Therefore, a fully-implicit nonlinear Newmark- $\beta$  numerical integration scheme is used to solve this second order initial value problem (Newmark, 1959). The average acceleration method, within the Newmark Scheme, is unconditionally stable, and uses the values  $\beta = 1/2$  and  $\gamma = 1/4$ . Adaptive time-stepping is exploited in the solver and the local error criteria  $\eta$  used here is given by (Zienkiewicz and Xie, 1991),

$$\eta = \|\mathbf{e}\| = \Delta t^2 (\beta - 1/6) \|\ddot{\mathbf{u}}_{k+1} - \ddot{\mathbf{u}}_k\| \quad (11)$$

Where  $k$  and  $k+1$  subscripts denote the previous and current time-steps, respectively. The solver is entirely implemented in an object-oriented MATLAB code.

## 5. MBS WHEEL-RAIL CONTACT

A rigid suspended wheelset is used along with rigid rails to extract the wheel-rail contact forces using the general-purpose MBS code **Sigma/Sams** (systematic integration of geometric modeling and analysis for the simulation of articulated mechanical systems). A three-dimensional non-conformal elastic contact algorithm is implemented to compute wheel-rail contact forces. The contact point coordinates on the wheels and the rail are obtained by solving a set of following nonlinear algebraic equations-  $(\mathbf{t}_1^r)^T (\mathbf{r}^w - \mathbf{r}^r) = 0$ ,  $(\mathbf{t}_2^r)^T (\mathbf{r}^w - \mathbf{r}^r) = 0$ ,  $(\mathbf{t}_1^w)^T \mathbf{n}^r = 0$ , and  $(\mathbf{t}_2^w)^T \mathbf{n}^r = 0$ . The superscripts  $w$  and  $r$  stand for the wheel and the rail respectively,  $\mathbf{r}^w$  and  $\mathbf{r}^r$  are the global position vectors of the potential contact point on the wheel and rail respectively,  $\mathbf{t}_1^w$  and  $\mathbf{t}_2^w$  are the tangents to the wheel surface at the contact point,  $\mathbf{n}^w$  is the normal to the wheel surface at the contact point,  $\mathbf{t}_1^r$  and  $\mathbf{t}_2^r$  are the two tangents to the rail, and  $\mathbf{n}^r$  is the normal to the rail. The wheel and rail surface parameters are obtained after solving these equations. The solution of these equations also ensures that the coordinates of the contact

point on the wheel and the rail surface are the same along the tangents  $\mathbf{t}_1^r$  and  $\mathbf{t}_2^r$ . The tangent planes are at the contact point are the same for the wheel and the rail surfaces. The contact equations can be written in a vector form as,  $\mathbf{C}^{w,r}(\mathbf{q}^r, \mathbf{q}^w, \mathbf{s}^r, \mathbf{s}^w, t) = \mathbf{0}$  where  $\mathbf{q}^r$  is the vector of generalized coordinates of the rail,  $\mathbf{q}^w$  is the vector of generalized coordinates of the wheel,  $\mathbf{s}^r$  is the vector of non-generalized coordinates or surface parameters of the rail, and  $\mathbf{s}^w$  is the vector of non-generalized coordinates or surface parameters of the wheel. Given the vectors of the generalized coordinates of the wheel and rail  $\mathbf{q}^w$  and  $\mathbf{q}^r$ , aforementioned equation can be solved for the surface parameters using an iterative Newton-Raphson method. The following equation is used for the Newton- Raphson iterations:

$$\left(\frac{\partial \mathbf{C}^{w,r}}{\partial \mathbf{s}^w}\right) \Delta \mathbf{s}^w + \left(\frac{\partial \mathbf{C}^{w,r}}{\partial \mathbf{s}^r}\right) \Delta \mathbf{s}^r = -\mathbf{C}^{w,r} \quad (12)$$

where,  $\Delta \mathbf{s}^w$  and  $\Delta \mathbf{s}^r$  are the Newton differences. Once the contact points are determined on the wheel and the rail, the normal contact force is computed based on the Hertzian approach

$$F^H = -K_H \delta^{3/2} - C_H \dot{\delta} |\delta| \quad (13)$$

where,  $K_H$  and  $C_H$  are the contact stiffness and damping coefficients, respectively, and  $\delta$  is the indentation (Shabana et al., 2004).

## 6. NUMERICAL RESULTS AND DISCUSSION

The railroad track substructure FE model described in Section 4 is used for the numerical analysis. Primarily two simulation scenarios are analyzed. In the first set of simulations, the ballast is modeled with linear elastic material properties, whereas the ballast is modeled using the cap plasticity model described in Sections 2 and 3 in the second set of simulations. Each set of simulations further considers the effect of contact force magnitude and the train traversing velocity on the geotechnical behavior of the rail substructure.

Mode shapes, modal frequency and stiffness values are derived from the elastic part of the finite element model. As the amount of plasticity in a given run is very small, the is a reasonable approximation (Foster and Kulkarni, 2021). After selecting a subset of the modes, the modes are truncated, so that only the nodal values associated with the rail nodes are used (El-Ghandour et al 2016). These are the only nodes needed for the multibody simulation, and hence the truncation results in a more efficient formulation. The multibody simulation is run in the time domain to determine the wheel-rail contact force, which is then applied back to the finite element simulation to determine plastic settlement.

### 6.1 Wheel-rail Contact Forces and Multibody Simulation



The MBS code, Sigma/Sams, is executed first to extract the wheel-rail contact forces. These forces are further applied on the flexible rails in the FE model as time-dependent boundary conditions. A rigid suspended wheelset is used with a vertically downward force to extract the transient history of the contact forces. Figure 10 shows the multibody model of the suspended wheelset. Whereas in Fig. 11, the time history of the wheel-rail contact force for average of 50 kN magnitude is shown. It can be seen that the transient effects in the initial stage of the simulation settle down and we obtain a steady-state contact response. The wheelset and rails are both considered as rigid bodies for the purposes of this investigation. As the number of loading cycles grows to a magnitude of hundreds of thousands, the plastic deformation of the ballast starts to affect the wheel-rail contact forces. The approach used in this paper will be able to use, as a part of future investigations, deformed rail substructure geometries with flexible MBS models to obtain the updated contact forces.

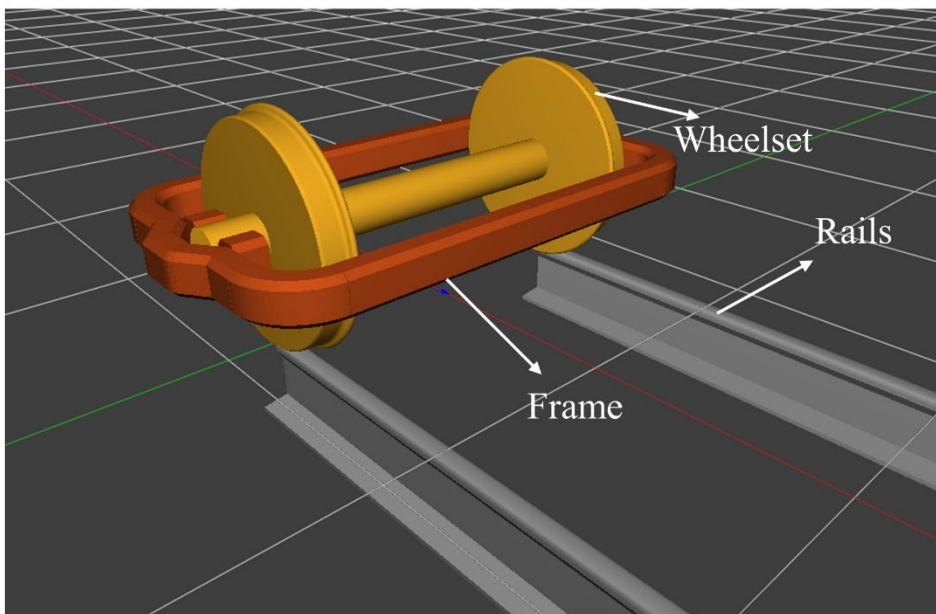


**Figure 10.** Multibody model of suspended wheelset

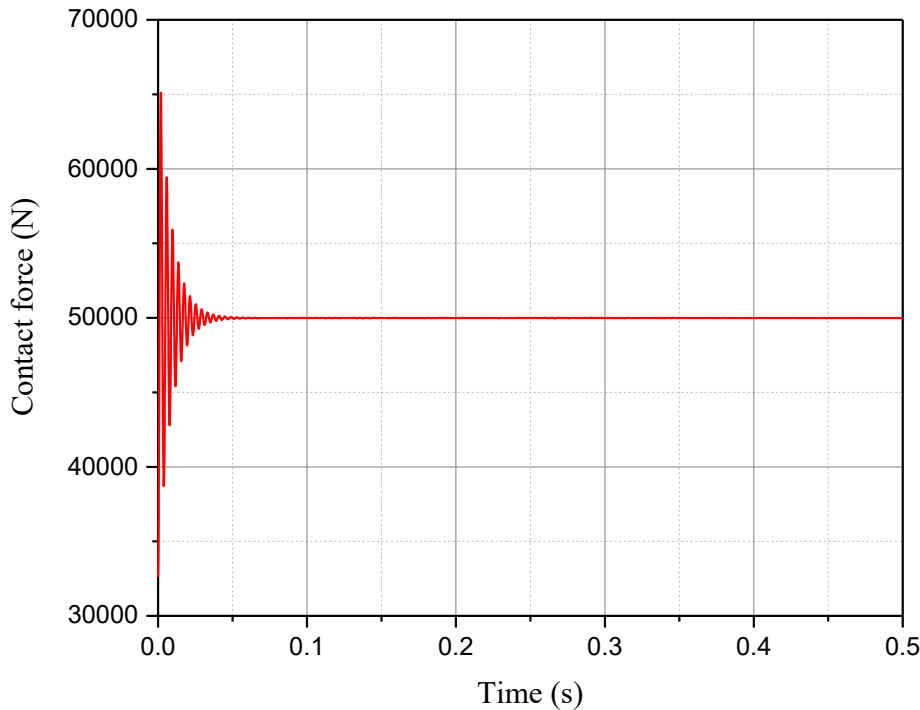


**Figure 11.** Wheel-rail contact force obtained from multibody model

## 6.2 Ballast with Linear Elastic Properties

In the first set of simulations, the ballast is modeled using linear elastic parameters from the material properties mentioned in Table 1. The primary goal of these simulations is to establish basic model verification. The effect of wheel-rail contact force magnitude and train traversing velocity on ballast displacement is studied. Two different values of mean contact force are used, 50 kN and 75 kN, along with two different values of train velocities, 77.76 km/hr and 25 km/hr, are used in the analysis. Table 3 shows a set of four simulations using the aforementioned force and velocity values with different permutations. Figure 12 shows the vertical displacement time history of a node directly beneath a rail on the second sleeper. Since all of the simulations in this case are fully elastic, no settlement is observed at the end. The highest vertical elastic displacement of -0.28 mm is observed for the third case where the mean contact force value is higher and the traversing velocity is lower, and the lowest displacement is observed for the fourth case where the contact force is lower and the velocity is higher. These results show that the vertical displacement increases with increase in the contact force value, and the displacement decreases with increase in the train velocity. This trend can be observed in Fig. 12 as well. The Poisson coupling in the soil lifts up the rails on both sides of the point of maximum displacement as observed in all four simulation cases. Figure 13 further shows the vertical displacement contours of the substructure when the wheel-rail force is exactly on top of the second and fourth sleepers, respectively, for the fourth case.

**Table 3.** Ballast sleeper node peak displacements – linear elastic simulations

Simulation #	Contact Force (kN)	Velocity (km/hr)	Peak Ballast Displacement (m)
1	50 (Low)	25 (Low)	-1.918E-04
2	75 (High)	77.8 (High)	-2.602E-04
3	75 (High)	25 (Low)	-2.877E-04
4	50 (Low)	77.8 (High)	-1.734E-04

The simulations with elastic ballast are used to gain confidence in the FE model used in this investigation. Recuero et al. (2011) is used as a reference to compare peak rail node displacements. The peak rail node displacement reported for undamaged track by Recuero et al. (2011) ranges from -0.36 mm to -0.41 mm, whereas the peak rail node displacement in case of the current investigation with similar parameters (Simulation 2) has a value of -0.25 mm. The higher displacements in case of Recuero et al. (2011) come from lower ballast stiffness value than that of the current investigation.

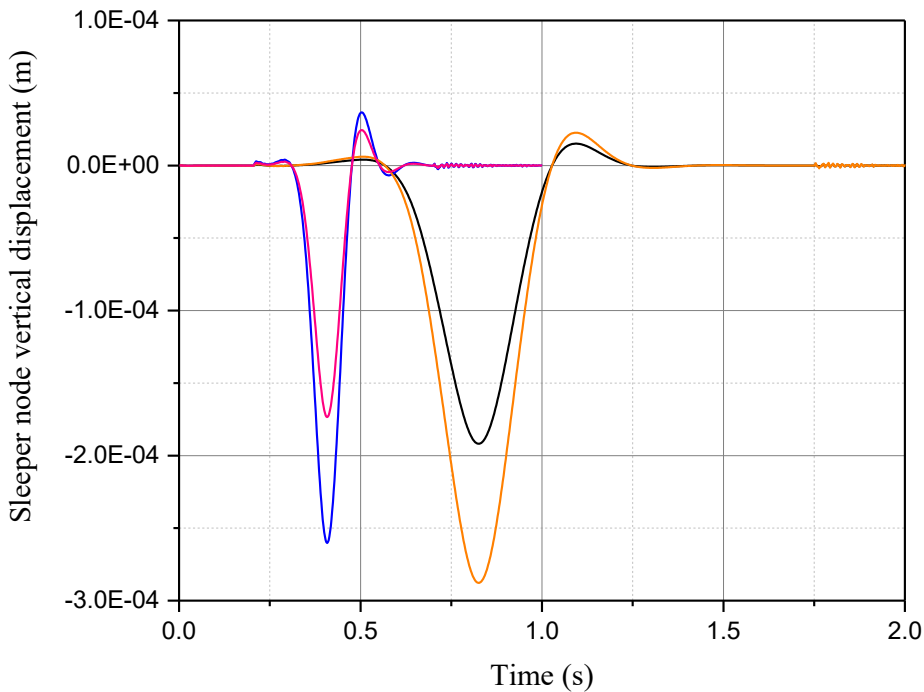


**Figure 12.** Sleeper 2 node vertical displacements for elastic ballast simulations

[Refer Table 3] ( Simulation 1, Simulation 2, Simulation 3, Simulation 4)

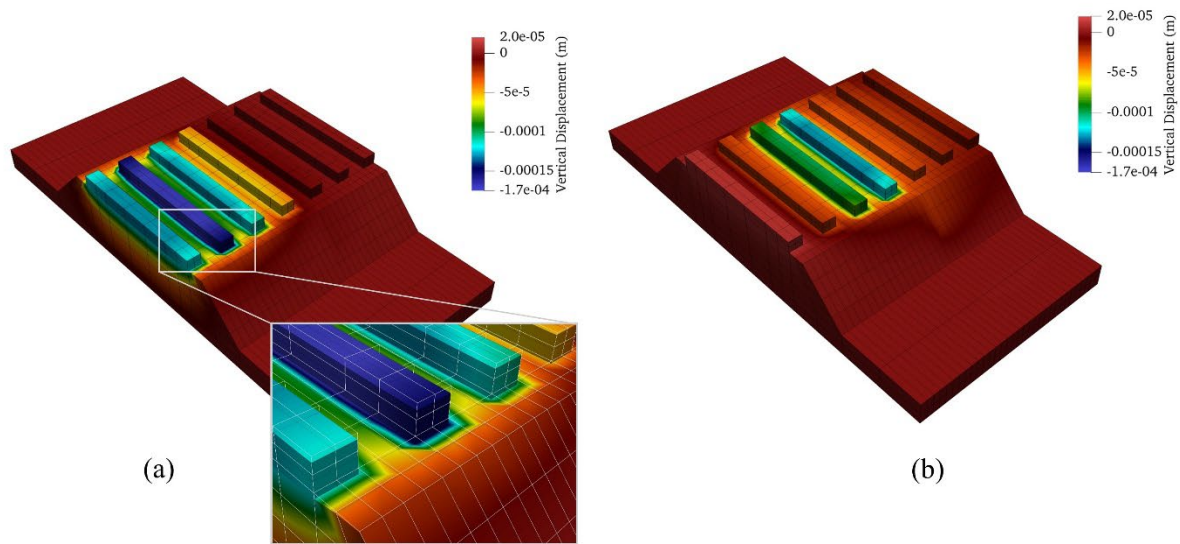


**Figure 13.** Vertical displacement contours – linear elastic ballast (a) Wheel-rail force on top of the second sleeper (b) Wheel-rail force on top of the fourth sleeper (Note: displacements magnified by a factor of 500 for illustration purposes)

### 6.3 Ballast with Cap Plasticity Material Model

In the second set of simulations, the ballast is divided into plastic and elastic regions to represent a stiffness transition, as shown in Fig. 7. The plastic region of the ballast has material properties specified in Table 1, and the rest of substructure components have material properties given in Table 2. Three different simulations are performed with different values of wheel-rail contact load and train velocity as done in the case of elastic ballast simulations, which are specified in Table 4.

For each combination of force and velocity, the evolution of plastic settlement of the ballast is studied at the end of three loading cycles. Each loading cycle consists of a single pass of the wheel-rail force along the entire track length. Figure 12 shows the vertical displacements of the nodes on the second and sixth sleepers for three loading cycles in case of all three simulations performed with inelastic ballast. Both of the nodes considered for this plot are directly underneath the rail. The second sleeper belongs to the plastic region of the ballast whereas the sixth sleeper is on top of the elastic concrete slab. For all four simulations, as the concrete slab has a higher stiffness value than the granular part of the ballast the second sleeper undergoes higher vertical displacements than that of the sixth sleeper. Figure 14 along with Table 4 analyze the effect of different wheel-rail contact load magnitudes and train velocities on the settlement. The highest displacement of -0.296 mm is observed for the second case where the mean contact force is high and traversing velocity is low, whereas the displacement is lowest for the first simulation where the force magnitude is low and the velocity magnitude is high. A similar trend is observed for the settlements, implying higher values of settlement are observed for

higher wheel-rail contact forces and lower train velocities. These observations further corroborate the findings presented by Tutumluer et al. (2007). The plastically settled nodes can be clearly observed for all three cases where the nodes settle at negative values specified in Table 4. The node belonging to the sixth sleeper shows no settlement in any case as the material response of the ballast beneath it is completely elastic. It can also be observed that the sleeper nodes are slightly lifted up before and after passage of wheel-rail force over them. Since the common nodes between the sleepers and the ballast share topology, the aforementioned phenomenon causes the settled sleepers to be pulled upwards by a small amount causing reduction in the settlement. As a part of future investigations, this shortcoming of the employed modeling technique will be alleviated by modeling the sleepers and the ballast as separate bodies with a contact interface between them, which allows separation as the sleepers displace away from the ballast. Figure 15 shows the plastic displacement of the ballast after three loading cycles for the second simulation case. As it can be observed, the settlement grows to maximum of 0.01 mm after three cycles of loading underneath the second sleeper. As the sleepers sink deeper in the ballast, the regions on the sides of the sleepers tend to protrude upwards, which is reflected in the red patches in the displacement contours shown in Fig. 15. This behavior is anticipated as the granular ballast particles beneath the sleepers are pushed away causing the particles on the sides and between the sleepers to rise up. The uneven settlements of the sleepers can be observed creating irregularities in the rail level. These irregularities grow as the substructure is subjected to numerous loading cycles, causing safety concerns and ride quality issues for the passing trains.

**Table 4.** Ballast settlement – simulations with plasticity

<b>Simulation #</b>	<b>Contact Force (kN)</b>	<b>Velocity (km/hr)</b>	<b>Peak Ballast Displacement (m)</b>	<b>Peak Settlement after 3 Loading Cycles (m)</b>
1	50 (Low)	77.8 (High)	-1.760E-04	-2.900E-06
2	75 (High)	25 (Low)	-2.963E-04	-1.000E-05
3	50 (Low)	25 (Low)	-1.958E-04	-5.300E-06

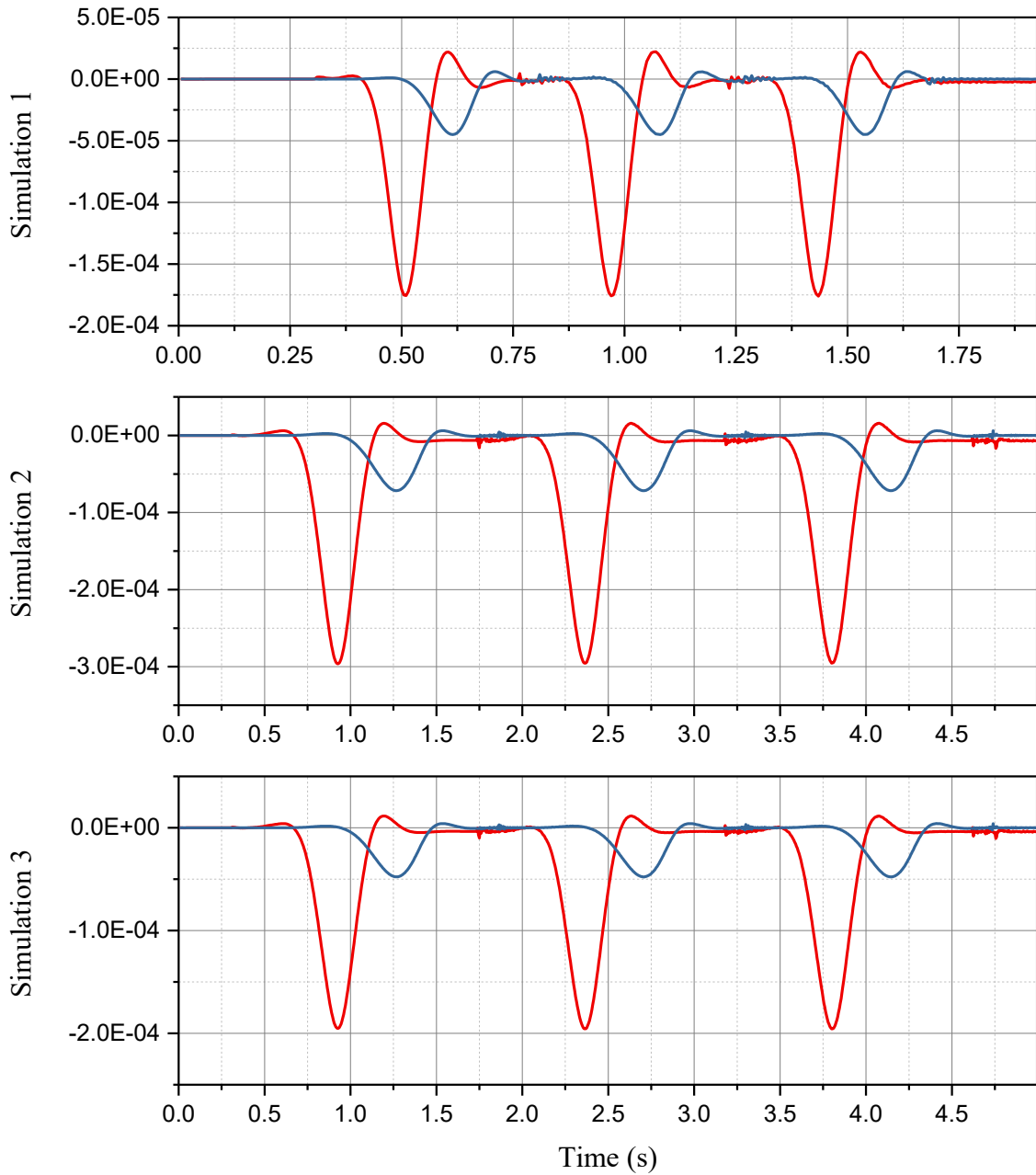


**Figure 14.** Sleeper node vertical displacements in meters

[Refer Table 4] ( Sleeper 2, Sleeper 6) —

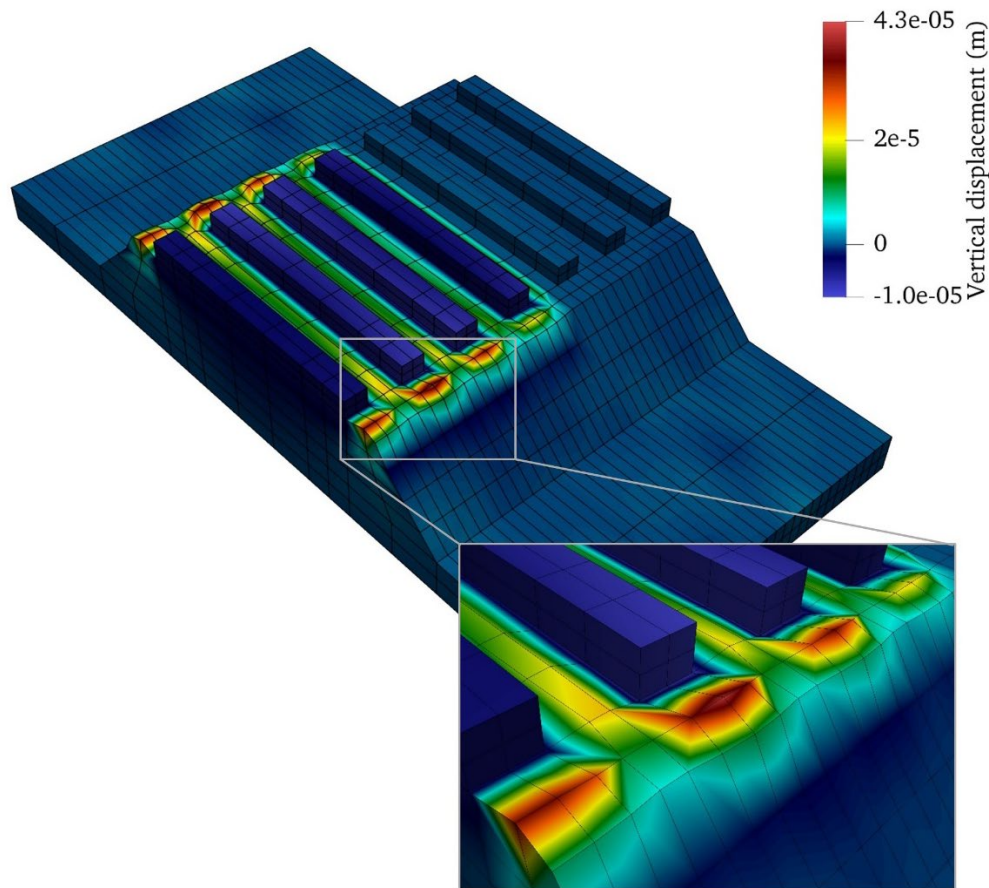


**Figure 15.** Settlement of the ballast after three loading cycles - Simulation 2 (Note: displacements magnified by a factor of 2000 for illustration purposes)

#### 6.4 Model Verification

In order to verify the FE model with inelasticity, results from Tutumluer et al. (2007) are considered. According to Tutumluer et al. (2007), for a wheel-rail contact force peak value of 120 kN and at a velocity of 28 km/hr, the settlement obtained after 20 loading cycles is approximately -0.08 mm. Therefore, linearly extrapolating the settlement value for three loading cycles comes out to be -0.012 mm. As for the current investigation, the peak settlement for contact force value of 75 kN and train velocity of 25 km/hr, the maximum settlement is observed to be around -0.01 mm, which closely matches to the findings in Tutumluer et al. (2007). The small difference between the two settlement values can be attributed to load and velocity magnitudes, geometry, modeling techniques and material parameters.

### 7. SUMMARY AND CONCLUSIONS

A comprehensive FE framework was created to analyze the behavior of the railroad track substructure under dynamic cyclic loading conditions. The inelastic behavior of the ballast material was modeled using a high-fidelity cap plasticity model, which has been previously validated in the literature. The plastic material properties of the ballast were characterized through extensive triaxial experimental tests. The ballast was divided into plastic and elastic regions to demonstrate the differential settlement in the areas where structural discontinuities are present. The geotechnical behavior of the ballast was analyzed for different values of wheel-rail contact force and train velocities. It was shown that the ballast is prone to settle more with higher values of contact force and lower magnitudes of train velocity. The uneven settlement of the sleepers belonging to the plastic and elastic parts of the ballast was shown for three loading cycles. As the settlement of the sleepers in the plastic section of the ballast grows, the uneven rails may cause decreased ride quality, and eventually safety issues. Therefore, this study has provided a new means to evaluate the railroad substructure behavior at a reasonable computational cost and high fidelity. The substructure behavior was also analyzed with linearly elastic considerations to show the effect of force and loading frequency on sleeper displacements. The elastic simulations were further used to verify the FE model used in this investigation. The FE structural dynamics solver was entirely implemented in an in-house MATLAB code with fully-implicit average acceleration method and adaptive time-stepping. In the future, the ballast-sleeper contact will be implemented to further demonstrate the effect of differential settlement, particularly creation of the ‘hanging sleepers’ scenario. This framework is also capable of coupling the FE analysis with flexible multibody dynamics algorithms to study the effect of settlement on wheel-rail contact forces. This strong coupling between multibody and FE codes can be achieved through following multiple steps. As a first step, the FE code can be used to extract the plastically settled geometry after several loading cycles. When the settlement is significant, the FE geometry can be exported to the multibody code by creating an equivalent floating frame of reference (FFR) formulation model. As the last step, the wheel-rail contact loads obtained from the multibody code can be exported to the FE to further extract the settlement. Therefore, aforementioned steps can be iterated until required number of loading cycles are achieved in the desired study. The use of ANCF beam elements facilitates easier geometry mapping between FE and MBS codes. These further investigations will significantly contribute towards safety of the railroad transport and optimization of the maintenance costs.



## REFERENCES

1. Dahlberg, T., 2001, "Some railroad settlement models - a critical review", *Proceedings of the Institution of Mechanical Engineers, Part F: Journal of Rail and Rapid Transit*, 215(4), pp.289-300.
2. Daocharoenporn, S., Mongkolwongrojn, M., Kulkarni, S. and Shabana, A.A., 2019, "Prediction of the pantograph/catenary wear using nonlinear multibody system dynamic algorithms", *Journal of Tribology*, 141(5).
3. El-Ghandour, A.I. and Foster, C.D., 2019, "Coupled finite element and multibody systems dynamics modelling for the investigation of the bridge approach problem", *Proceedings of the Institution of Mechanical Engineers, Part F: Journal of Rail and Rapid Transit*, pp.00.
4. El-Ghandour, A.I., Hamper, M.B. and Foster, C.D., 2016, "Coupled finite element and multibody system dynamics modeling of a three-dimensional railroad system", *Proceedings of the Institution of Mechanical Engineers, Part F: Journal of Rail and Rapid Transit*, 230(1), pp.283-294.
5. Ford, R., 1995, "Differential ballast settlement, and consequent undulations in track, caused by vehicle-track interaction", *Vehicle System Dynamics*, 24(sup1), pp.222-233.
6. Fossum, A. F. and Brannon, R. M., 2004, The Sandia GeoModel: theory and user's guide, Report, Sandia National Laboratories.
7. Foster, C.D., and Kulkarni, S., *Coupled Multibody and Finite Element Modelling of Track Settlement*. 16th International Conference of the International Association for Computer Methods and Advances in Geomechanics, May 5-8, 2021, Turin, Italy
8. Foster, C.D., Regueiro, R.A., Fossum, A.F. and Borja, R.I., 2005, "Implicit numerical integration of a three-invariant, isotropic/kinematic hardening cap plasticity model for geomaterials", *Computer Methods in Applied Mechanics and Engineering*, 194(50-52), pp.5109-5138.
9. Gerstmayr, J., and Shabana, A. A., 2006, "Analysis of thin beams and cables using the absolute nodal co-ordinate formulation", *Nonlinear Dynamics*, 45(1-2), pp. 109-130.
10. Grossi, E. and Shabana, A.A., 2018, "ANCF analysis of the crude oil sloshing in railroad vehicle systems", *Journal of Sound and Vibration*, 433, pp.493-516.

11. Hamed, A.M., Jayakumar, P., Letherwood, M.D., Gorsich, D.J., Recuero, A.M. and Shabana, A.A., 2015, "Ideal compliant joints and integration of computer aided design and analysis", *Journal of Computational and Nonlinear Dynamics*, 10(2), p.021015.
12. Huang, H., Shen, S. and Tutumluer, E., 2010, "Moving load on track with Asphalt trackbed", *Vehicle System Dynamics*, 48(6), pp.737-749.
13. Huang, H. and Tutumluer, E., 2011, "Discrete element modeling for fouled railroad ballast", *Construction and Building Materials*, 25(8), pp.3306-3312.
14. Indraratna, B. and Nimbalkar, S., 2013, "Stress-strain degradation response of railway ballast stabilized with geosynthetics", *Journal of geotechnical and geoenvironmental engineering*, 139(5), pp.684-700.
15. Indraratna, B., Thakur, P.K. and Vinod, J.S., 2009, "Experimental and numerical study of railway ballast behavior under cyclic loading", *International Journal of Geomechanics*, 10(4), pp.136-144.
16. Jiang, Y. and Nimbalkar, S.S., 2019, "Finite Element Modelling of Ballasted Rail Track Capturing Effects of Geosynthetic Inclusions", *Frontiers in Built Environment*, 5, p.69.
17. Kaewunruen, S. and Mirza, O., 2017, "Hybrid Discrete Element-Finite Element Simulation for Railway Bridge-Track Interaction", *IOP Conference Series: Materials Science and Engineering*, 251(1), pp. 012016.
18. Kalker, J.J., 1996, "Discretely supported rails subjected to transient loads", *Vehicle System Dynamics*, 25(1), pp.71-88.
19. Kulkarni, S., Pappalardo, C.M. and Shabana, A.A., 2017, "Pantograph/catenary contact formulations", *Journal of Vibration and Acoustics*, 139(1), p.011010.
20. Kulkarni, S. and Shabana, A.A., 2019, "Spatial ANCF/CRBF beam elements", *Acta Mechanica*, 230(3), pp.929-952.
21. Li, X., Nielsen, J.C. and Pålsson, B.A., 2014, "Simulation of track settlement in railway turnouts", *Vehicle System Dynamics*, 52 (sup1), pp.421-439.
22. Lu, M. and McDowell, G.R., 2010, "Discrete element modelling of railway ballast under monotonic and cyclic triaxial loading", *Géotechnique*, 60(6), p.459.
23. Lundqvist, A. and Dahlberg, T., 2005, "Load impact on railway track due to unsupported sleepers", *Proceedings of the Institution of Mechanical Engineers, Part F: Journal of Rail and Rapid Transit*, 219(2), pp.67-77.
24. Mahmoud, E., Papagiannakis, A.T. and Renteria, D., 2016, "Discrete element analysis of railway ballast under cycling loading", *Procedia engineering*, 143, pp.1068-1076.

25. Mauer, L., 1995, "An interactive track-train dynamic model for calculation of track error growth", *Vehicle System Dynamics*, 24(sup1), pp.209-221.
26. Motamedi, M.H., 2016, "Numerical Simulation of Mechanical Response of Geomaterials from Strain Hardening to Localized Failure", PhD Thesis, University of Illinois at Chicago.
27. Motamedi, M.H. and Foster, C.D., 2015, "An improved implicit numerical integration of a non-associated, three-invariant cap plasticity model with mixed isotropic–kinematic hardening for geomaterials", *International Journal for Numerical and Analytical Methods in Geomechanics*, 39(17), pp.1853-1883.
28. Newmark, N.M., 1959, "A method of computation for structural dynamics", *American Society of Civil Engineers*.
29. Nishiura, D., Sakaguchi, H. and Aikawa, A., 2017, "Development of viscoelastic multi-body simulation and impact response analysis of a ballasted railway track under cyclic loading", *Materials*, 10(6), pp.615-636.
30. Patel, M., Orzechowski, G., Tian, Q. and Shabana, A.A., 2016, "A new multibody system approach for tire modeling using ANCF finite elements", *Proceedings of the Institution of Mechanical Engineers, Part K: Journal of Multi-body Dynamics*, 230(1), pp.69-84.
31. Recuero, A.M., Escalona, J.L. and Shabana, A.A., 2011, "Finite-element analysis of unsupported sleepers using three-dimensional wheel–rail contact formulation", *Proceedings of the Institution of Mechanical Engineers, Part K: Journal of Multi-body Dynamics*, 225(2), pp.153-165.
32. Sato, Y., 1997, Optimization of track maintenance work on ballasted track, Proceedings of the world congress on railway research (WCRR'97), Florence, Italy.
33. Schanz, T., Vermeer, P.A. and Bonnier, P.G., 1999, "The hardening soil model: formulation and verification", *Beyond 2000 in computational geotechnics*, pp.281-296.
34. Shabana, A.A., Zaazaa, K.E., Escalona, J.L. and Sany, J.R., 2004, "Development of elastic force model for wheel/rail contact problems", *Journal of sound and vibration*, 269(1-2), pp.295-325.
35. Sutley, G.H., 2009, "Finite element analysis of soil under explosive loading", PhD Thesis, University of Colorado at Boulder.
36. Tutumluer, E., Hashash, Y., Ghaboussi, J., Qian, Y., Lee, S.J. and Huang, H., 2018, "Discrete Element Modeling of Railroad Ballast Behavior", Report-No. DOT/FRA/ORD-18/20.
37. Tutumluer, E., Huang, H., Hashash, Y.M.A. and Ghaboussi, J., 2007, Discrete element modeling of railroad ballast settlement, *AREMA Annual Conference*, Chicago, United States of America.

38. Tutumluer, E., Qian, Y., Hashash, Y.M., Ghaboussi, J. and Davis, D.D., 2013, “Discrete element modelling of ballasted track deformation behavior’, *International Journal of Rail Transportation*, 1(1-2), pp.57-73.
39. Zienkiewicz, O.C. and Xie, Y.M., 1991, “A simple error estimator and adaptive time stepping procedure for dynamic analysis”, *Earthquake engineering & structural dynamics*, 20(9), pp.871-887.